NIH Public Access
Author Manuscript
Chem Res Toxicol. Author manuscript; available in PMC 2013 January 13.

Published in final edited form as:
Chem Res Toxicol. 2012 January 13; 25(1): 15–34. doi:10.1021/tx200339h.

Biological Interactions of Graphene-Family Nanomaterials – An Interdisciplinary Review

Vanesa C. Sanchez[+], **Ashish Jachak**[+], **Robert H. Hurt**[*,Ψ,#], and **Agnes B. Kane**[*,+,#]
Department of Pathology and Laboratory Medicine, Brown University, Providence, Rhode Island 02912, United States, School of Engineering, Brown University, Providence, Rhode Island 02912, United States, and Institute for Molecular and Nanoscale Innovation, Brown University, Providence, Rhode Island, 02912, United States

Abstract

Graphene is a single-atom thick, two-dimensional sheet of hexagonally arranged carbon atoms isolated from its three-dimensional parent material, graphite. Related materials include few-layer-graphene (FLG), ultrathin graphite, graphene oxide (GO), reduced graphene oxide (rGO), and graphene nanosheets (GNS). This review proposes a systematic nomenclature for this set of "Graphene-Family Nanomaterials" (GFNs) and discusses specific materials properties relevant for biomolecular and cellular interactions. The article discusses several unique modes of interaction between GFNs and nucleic acids, lipid bilayers, and conjugated small molecule drugs and dyes. Some GFNs are produced as dry powders using thermal exfoliation, and in these cases inhalation is a likely route of human exposure. Some GFNs have aerodynamic sizes that can lead to inhalation and substantial deposition in the human respiratory tract, which may impair lung defense and clearance leading to formation of granulomas and lung fibrosis. The limited literature on *in vitro* toxicity suggests that GFNs can be either benign or toxic to cells, and it is hypothesized that the biological response will vary across the material family depending on layer number, lateral size, stiffness, hydrophobicity, surface functionalization, and dose. Generation of reactive oxygen species (ROS) in target cells is a potential mechanism for toxicity, although the extremely high hydrophobic surface area of some GFNs may also lead to significant interactions with membrane lipids leading to direct physical toxicity or adsorption of biological molecules leading to indirect toxicity. Limited *in vivo* studies demonstrate systemic biodistribution and biopersistence of GFNs following intravenous delivery. Similar to other smooth, continuous, biopersistent implants or foreign bodies, GFNs have the potential to induce foreign body tumors. Long-term adverse health impacts must be considered in design of GFNs for drug delivery, tissue engineering, and fluorescence-based biomolecular sensing. Future research is needed to explore fundamental biological responses to GFNs including systematic assessment of the physical and chemical materials properties related to toxicity. Complete materials characterization and mechanistic toxicity studies are essential for safer design and manufacturing of GFNs in order to optimize biological applications with minimal risks for environmental health and safety.

[*]To whom correspondence should be addressed: Robert H. Hurt, School of Engineering, Brown University, Box H, Providence, Rhode Island 02912, United States, Telephone: 401-863-2685, Fax: 401-863-9120, Robert_Hurt@Brown.edu. Agnes B. Kane, Department of Pathology and Laboratory Medicine, Brown University, Box G-E5, Providence, Rhode Island 02912, United States, Telephone: 401-863-1110, Fax: 401-863-9008, Agnes_Kane@Brown.edu.
[+]Department of Pathology and Laboratory Medicine
[Ψ]School of Engineering
[#]Institute for Molecular and Nanoscale Innovation
Vanesa C. Sanchez and Ashish Jackak contributed equally to this review.

NIH-PA Author Manuscript
NIH-PA Author Manuscript
NIH-PA Author Manuscript

NIH-PA Author Manuscript

NIH-PA Author Manuscript

NIH-PA Author Manuscript

1. Introduction

The responsible development of nanotechnology will require a coordinated and sustained research effort to understand and manage its risks for human health and the environment. Current nanosafety research is focusing primarily on a small set of materials that are likely to be manufactured at high production volume, and may thus be associated with significant human or environmental exposures. Recently there has been an explosion of interest in a new nanomaterial, first discovered in 2004, but already worthy of inclusion in this set: graphene. Graphene is a single-atom-thick, two-dimensional sheet of hexagonally arranged carbon atoms, whose isolation from crystalline graphite and characterization [1] led to the Nobel Prize in 2010. The number of scientific papers on graphene exceeded 3000/yr in 2010 (Web-of-Science topical area search), and a number of companies have formed worldwide that manufacture and sell graphene, albeit at this time primarily for research and development.

Much of the excitement in graphene research centers on its nanoelectronics applications where it is used as a single-atom-thick coating on substrates that can be patterned into transistors or other logic circuit elements as the basis for next-generation computing or sensing [2]. In this form, as a bound or imbedded microchip component, graphene is unlikely to pose a significant environmental or health risk. As graphene research has expanded, however, other engineering applications have emerged, such as structural composites [3], conducting polymers [3], battery electrodes [4, 5], supercapacitors [6], transport barriers [7,8], printable inks [9], antibacterial papers [6], and biomedical technologies, [3, 10, 11] where exposures are much more likely. These diverse applications have led to interest in manufacturing not only substrate-bound extended graphene monolayers, but also related materials that include few-layer-graphene (FLG), ultrathin graphite, graphene oxide (GO), reduced graphene oxide (rGO), and graphene nanosheets (GNS). The present article focuses on this broad set of “Graphene-Family Nanomaterials” (GFNs), in order to represent the range of materials to which humans or environmental receptors may ultimately be exposed.

The literature on the biological interactions of graphene family nanomaterials is growing rapidly, and includes studies primarily motivated by (i) biomedical applications, and (ii) environmental health and safety (EHS). As with other nanomaterials, the issue of potential toxicity arises not only in biomedical applications, but also in non-biomedical products where unintended occupational, consumer, and environmental exposures can occur. The biomedical applications of GFNs are just emerging, and have been reviewed recently by Feng and Liu [12]. There is also a significant literature on graphene-based biochemical sensing, based on GFNs as fluorescence quenchers or electrode materials. These areas have been reviewed recently by Shao *et al.* [13] and Kuila *et al.* [14], and will not be covered in detail here.

The biomedical and EHS fields share a common scientific goal: to understand the fundamental interactions of new ultrathin carbon forms with biological molecules, tissue structures, and organisms. The present article reviews the literature on the graphene-biological interface with emphasis on mechanisms and the fundamental biological responses relevant both to applications and to material safety. Throughout the article we emphasize the variations in properties and behaviors within the broader graphene nanomaterial family, and the potential for these variations to produce different biological responses, which if understood, could be intelligently exploited for function or safety.

2. The Graphene Nanomaterial Family

Graphene materials vary in layer number, lateral dimension, surface chemistry, defect density or quality of the individual graphene sheets, and composition or purity. In this way

NIH-PA Author Manuscript

NIH-PA Author Manuscript

NIH-PA Author Manuscript

GFNs are analogous to carbon nanotubes, which vary in wall number, diameter, length, surface chemistry and the amount, composition, and physical form of metal impurities. Figure 1 shows the most important GFNs and some structural features relevant for colloidal behavior and biological interactions. The sections below define the larger set of materials encountered in practice, which are variations on the basic chemical structures shown in Figure 1.

Monolayer graphene, or "graphene" is the material that has attracted the most interest due to its unique electronic properties [15]. Graphene can be isolated from graphite by repeated "mechanical exfoliation" of graphite flakes using adhesive tape [1] or grown on substrates for electronics applications by chemical vapor deposition or decomposition of carbide phases [16], where it is of secondary interest for this review on biological effects. It can also be a clamped free-standing film or ribbon [16] or can be suspended in solvents either with surfactants [17] or without [18], where it is of somewhat more relevance here. Pristine graphene of significant lateral dimension is difficult to isolate in the gas phase and also difficult to suspend in solvents at high concentration, so most of the interest in biological applications and implications is focused on the related materials described in the sections below.

Few-layer graphene (FLG) is defined here as flake-like stacks of 2–10 graphene layers. It was originally a byproduct of, or precursor in, the fabrication of monolayer graphene [1], but has become an interesting commercial material in its own right. Introduction of sulfate, nitrate, or other ions between the layers of crystalline graphite (intercalation) followed by rapid thermal heating, leads to internal pressure buildup and massive expansion of the layered structure of natural graphite. This "thermal exfoliation" produces dry powders, which can be dispersed into FLG samples that become reinforcing agents in composite materials, or further processed into graphene or graphene oxide. The dry powder product may contain residual intercalants, often sulfur compounds, and offers the possibility of occupational exposure in high-temperature furnace operations not unlike those for carbon nanotubes. The raw product of the thermal exfoliation can be referred to as "expanded graphite" and its precursor, the graphite material with the intercalant loaded inside is sometimes referred to as "expandable graphite", since it can be heated to produce "expanded graphite" and processed into FLG or other GFNs.

Ultrathin Graphite is defined here as material with thickness greater than 10 sheets (3–5 nm) but less than 100 nm. With this definition, ultrathin graphite is classified as a nanomaterial by the U.S. National Science Foundation, being a material with at least one dimension in the range 1–100 nm. In terms of thickness, there is a continuum of material structures from monolayer graphene to conventional graphite powders, and it is attractive to define ultrathin graphite in this way lying between FLG and milled graphite powders of larger minimum dimension, which are not classified as "nanomaterials".

Graphene oxide (GO) is a highly oxidized form of chemically modified graphene, produced by harsh oxidation of crystalline graphite followed by sonication or other dispersion methods to produce monolayer material, typically in aqueous suspension [18]. The structure of GO (Figure 1) consists of single-atom-thick carbon sheets with carboxylate groups on the periphery, where they provide pH dependent negative surface charge and colloidal stability [18]. The basal surfaces contain hydroxyl (-OH) and epoxide (-O-) functional groups, which are uncharged but polar. The basal planes also include unmodified graphenic domains that are hydrophobic and capable of π-π interactions relevant to adsorption of dye molecules or some drugs (vida infra). The result is an amphiphilic giant sheet-like molecule that can act like a surfactant [19] and stabilize hydrophobic molecules in solution, or collect at interfaces [20, 21]. GO samples may contain not only monolayers but also multilayer flakes, and a full characterization of the material requires a layer number

NIH-PA Author Manuscript

NIH-PA Author Manuscript

NIH-PA Author Manuscript

distribution, which is difficult to measure, however, and is seldom reported. For applications requiring monolayers, centrifugation is typically employed to remove material not fully exfoliated into single-atom-thick sheets.

Reduced graphene oxide (rGO) is the product of treating GO under reducing conditions, which include high-temperature thermal treatment and chemical treatments with hydrazine (N_2H_4) or other reducing agents [18]. The goal of GO reduction is often done to restore electrical conductivity, and it alters many other GO properties as well. It reduces oxygen content, increases hydrophobicity, introduces holes or defects in the carbon lattice due to CO/CO_2 liberation [22], and reduces surface charge and water dispersibility.

Nano-GO is a term sometimes used to describe graphene oxide of small lateral dimension, typically less than 100 nm and often below 20 nm. These materials have typically been used in biological applications, because small size facilitates cell entry and dispersion stability. Some authors use Graphene NanoSheets (GNS), though this can be misleading since the basic chemistry is often that of graphene oxide not graphene. Neither nano-GO nor GNS are a necessary part of the graphene family terminology, since lateral dimension must be specified already to fully define any graphene material, but is nevertheless convenient to distinguish these very small materials from the extended lateral dimension materials that are the goal of most synthesis efforts.

For the remainder of this review, we will systematically use the terms defined above when describing individual studies, and where possible, describe the materials more specifically in terms of layer number, lateral dimension, and surface chemistry.

3. Material Properties Relevant to Biological Effects

The properties of GFNs most relevant for their biological effects include surface area, layer number, lateral dimension, surface chemistry, and purity.

3.1 Surface area

Surfaces play a central role in the biological interactions of nanomaterials [23]. It is often pointed out that small nanoparticles (< 10 nm) have a significant fraction of their atoms exposed on their surfaces. Monolayer graphene represents an extreme case, in which *every atom* lies on the surface, and in fact each atom is exposed to the surrounding medium on two sides, giving rise to the theoretical maximum surface area of an sp^2-hybridized carbon sheet of about 2600 m^2/g. This is at least an order of magnitude higher than the surface area of most other nanomaterials studied in biological systems. Monolayer graphene oxide has a very similar area, but its surface is modulated by atomic-scale roughness. The surface areas of other GFNs decrease as layer number increases (see next section).

Because of the high surface area of GFNs, especially monolayer graphene and GO, we anticipate that surface phenomena, either physical adsorption or catalytic chemical reaction, will be particularly important in the biological response to these materials. The closest analogue to graphene is a pristine single-walled carbon nanotube (SWNT), which has a theoretical outer surface area of 1300 m^2/g, and is similarly hydrophobic, though in many cases in practice this surface area is significantly reduced by bundling to values below 500 m^2/g. The high hydrophobic area of SWNTs has been associated with the adsorption of molecular probe dyes and *in vitro* artifacts [24, 25], and the depletion of folic acid and other micronutrients from cell culture medium leading to cell growth inhibition [26]. Adsorptive interferences have also been reported for carbon black [27] and are expected for other materials with large hydrophobic surface area like GFNs. The high surface areas of GFNs

NIH-PA Author Manuscript

NIH-PA Author Manuscript

NIH-PA Author Manuscript

make surface reactions potentially important, including ROS production, antioxidant deactivation [28], or ROS quenching [29].

GFNs raise an interesting issue of surface area stability in biological experiments. When spherical particles aggregate in medium, their effective size increases, but they typically retain most of their surface area, which represents the perimeters of the primary particles in the aggregate (Figure 2). Hard spheres make only point contacts, and thus most surface area is retained during sphere-to-sphere aggregation, unless the aggregates partially fuse by sintering or dissolution/re-precipitation. Plates, however, often pack face-to-face and much of the surface area in a plate-like colloid may be irreversibly lost by aggregation, or by processes such as filtration or centrifugation (Figure 2). GO in particular is reported to align effectively during filtration or drying to make GO papers, and after stacking the interlayer spaces are not typically accessible for biological interactions or accessible to vapor phase probes used to measure surface area, unless a second component is added to form high-area "pillared" GO [30]. The effective or measurable surface area may thus change significantly during sample preparation or biological testing. For many GFNs, it will not be possible to make meaningful measurements of surface area in a biological system by the conventional method of drying/filtering and applying vapor adsorption methods and the BET equation, as the drying/filtration process likely eliminates the area one seeks to measure.

Another aspect of the plate-like geometry of GFNs is their tendency to block filters by deposition with the plane of the plate parallel to the substrate, making separation by ultrafiltration slow and tedious. A final aspect is the inability to quantitatively characterize their size and shape by conventional dynamic light scattering techniques, which use spherical particle models to compute size and zeta potential from raw data on scattered light intensity.

3.2 Layer number

The number of graphene layers in a GFN is important because it determines specific surface area and bending stiffness (Figure 3). Simple geometric considerations for large thin plates give $A/m = 2/\rho d$, where A/m is the total area per unit mass, ρ is the material density and d is the thickness given by $N_{layer}d_1$, where is the layer number and d_1 the thickness of a single layer, 0.34 nm for unoxidized FLG. Combining gives:

$$A/m=2/\rho N_{layer}d_1 \quad (1)$$

Which shows that the specific area (m^2/g) is inversely proportional to layer number (Figure 3). It is expected that the adsorptive capacity for biological molecules will increase significantly as layer number decreases. Stiffness is reported to be important in the pathological response to fibers and carbon nanotubes [31] but its role in plate-like materials is unknown. The thinnest materials, e.g. monolayer graphene or GO, are quite deformable by weak forces such as water surface tension [21, 32, 33]. The multilayer materials in contrast may act as rigid bodies during their cellular interactions (see micrograph in Figure 10). Figure 3 also shows bending stiffness values calculated from the elastic modulus for monolayer graphene and the area moment of inertia for multilayer films of varying thickness. Stiffness increases with the third power of layer number or material thickness. Characterization of layer number typically involves deposition on substrates followed by AFM or optical absorbance measurements, or for FLG samples by estimation from measured surface areas using equation (1).

NIH-PA Author Manuscript

NIH-PA Author Manuscript

NIH-PA Author Manuscript

3.3 Lateral dimension

Lateral dimension has no significant effect on specific surface area (m^2/g), but does determine the maximum dimension of the material, which is relevant for cell uptake, renal clearance, blood-brain barrier transport and many other biological phenomena that depend on particle size. The cellular uptake of plate-like nanostructures is poorly understood, but will likely be sensitive to lateral dimension, which represents the maximum dimension of the object undergoing endocytosis or phagocytosis. Lateral dimension should affect the population of receptors needed for uptake, and also the size of the endosome or lysosome into which the material must be packaged within the cell. The lateral sizes of GFNs span orders of magnitude, from nano-GO at 10 nm (the size of some proteins) to > 20 μm (larger than most cells). Cells may thus adhere and spread (for larger GFNs), or successfully internalize the plates (for smaller GFNs), or experience some form of frustrated endocytosis or phagocytosis with implications for biological risk. Lateral dimension also influences deformability (along with layer number), but the lateral dimension also determines the torque that can be applied by cellular forces. Laterally large plates are more deformable than small plates at equal layer number. Characterization of lateral dimension typically involves deposition on substrates such as oxidized silicon followed by SEM or AFM and statistical image analysis.

3.4 Surface chemistry

The graphene family includes materials with widely varying surface chemistry, even before any specific biofunctionalization is carried out. Graphene oxide surfaces are partially hydrophobic with hydrophilic (typical water contact angle 40–50 degrees) regions [34, 35] capable of hydrogen bonding and metal ion complexing [36], and contain negative charges on edge-sites associated with carboxylate groups [37]. The pristine graphene surface, in contrast, is hydrophobic (water contact angle near 90°) and capable of biochemical reactions primarily at edge or defect sites. Reduced graphene oxide is intermediate in hydrophilicity and in basal reactivity, since it contains basal vacancy defects produced during oxygen removal [22]. Much of the biomedical work has been done on nanoscale graphene oxide due to its higher dispersibility in aqueous phases. Although GO colloids in pure water can be quite stable, long-term stability in saline or culture medium has been reported to require further functionalization [12, 38]. Pristine graphenes (monolayer or FLG) are very poorly dispersible in water and require surfactants or other stabilizing agents for any meaningful application requiring suspension in biological fluids. Recent experience with CNTs has shown that most synthetic surfactants are problematic due to toxicity, and instead the field has developed protein, serum, or lipid coating methods for biocompatible dispersion [39], and these same techniques may prove useful for pristine surface GFNs.

3.5 Purity

Unlike CNTs, GFNs are not typically grown catalytically and do not contain residual metal catalysts. However, some GFNs may contain residual intercalants, chemical additives used to separate the layers in the bulk graphite feedstock and have not been fully removed by washing. Graphene oxide synthesis uses a variety of reagents that may leave soluble residues in the suspension if they are not properly washed, and the washing of GO can be tedious due to gellation caused by physical interaction of the giant molecular disks [20]. The reagents used in various GFN syntheses include permanganate, nitrate, sulfate, chromate, peroxide, persulfate, hydrazine and borohydride and associated cations, typically potassium, sodium, or ammonium. There is little known about the biological effects of impurities in GFNs, but caution and careful material characterization are advised, as always when carrying out biological effects studies.

NIH-PA Author Manuscript

NIH-PA Author Manuscript

NIH-PA Author Manuscript

4. Biomolecular Interactions

This section reviews the rapidly growing literature on the fundamental interactions of GFNs with biological molecules, including small molecule drugs, metal ions, nucleic acids, lipids, and proteins.

4.1 Small molecule and ion adsorption

One of the defining characteristics of graphene materials is high surface area, and GFNs can be expected to be potent sorbents for a variety of small molecule solutes in physiological fluids. Adsorption on carbon surfaces is generally favored for molecules with low solubility, partial hydrophobicity, or positive charge (for the common case of negatively charged GFNs), and for molecules with conjugated π-bonds that impart planarity and allow π-π interactions with graphenic carbon surfaces. The biological consequences may include (i) micronutrient depletion [26], (ii) artifacts in assays that rely on dye-based molecular probes [24, 25], (iii) the capacity to carry small molecule drug cargoes [40], and (iv) synergistic or antagonistic toxic effects when GFMs coexist with small molecule toxicants, whose bioavailabilty can be increased or decreased as they partition to graphene surfaces.

Most of the attention on small molecule interactions has been related to drug delivery, where GFNs and nano-GO in particular are used as carriers for small molecular agents. Sun *et al.* [38] loaded the commercial chemotherapeutic agent doxorubicin on PEGylated nano-GO, where the pegylation density is presumed to be low enough that sp^2 domains remain available on the GO surface for drug binding. Doxorubicin (Dox) was reported to adsorb by π-stacking and to desorb at reduced pH due to its higher hydrophilicity and high solubility at an intracellular endosomal pH of 5.5. We can anticipate that other drug molecules with titratable amine groups may also show this higher solubility and partial reversibility at low intracellular pH due to increased positive charge. Dox is a planar conjugated molecule that exerts its chemotherapeutic effect through DNA intercalation, a behavior that might be shared with nano-GO itself (see below). Huang *et al.* [41] loaded the photosensitizer chlorin e6 (Ce6) onto microscale GO surfaces for targeted photodynamic therapy. The highly conjugated Ce6 is reported to adsorb by hydrophobic forces and π-π stacking, implying that it occurs in the unsubstituted graphenic clusters that lie between the oxygen functional groups on GO surfaces. Zhang *et al.* [10] loaded both Dox and camptothecin (CPT) onto functionalized nano-GO, and again cite π-π interactions and hydrophobic forces as the driving force for adsorption. Overall, nano-GO and its functionalized versions are effective sorbents for carrying hydrophobic compounds in biological systems, which is related to the reported amphiphilicity of GO [19] with its patchwork of oxygenated and unsubstituted graphenic surfaces.

To our knowledge there are no published studies of molecular dye or probe adsorption by GFNs or associated interferences with *in vitro* toxicological assays. There has been an environmentally motivated study of methylene blue adsorption that reports very high capacities for this common dye [42], and there is some information on GFN dye quenching through adsorption or diffusive quenching [43, 44], but the implications for biological *in vitro* testing remain unknown and are worthy of future study.

Exogenous or endogenous metal ions may be adsorbed by GO, nano-GO and to some extent rGO by complexation or chelation on oxygen functional groups. This effect has been reported for Mg^{2+} [45], and Cu^{2+} [36, 46]. The copper ion adsorption is reported to mediate the interaction of nano-GO with DNA (see section on DNA interactions).

NIH-PA Author Manuscript

NIH-PA Author Manuscript

NIH-PA Author Manuscript

4.2 Nucleic acid interactions

The most active area of research on GFN biomolecular interactions involves DNA/RNA [46–49]. GFNs show several unique modes of interaction with DNA/RNA that include preferential adsorption of single-stranded (ss) over double stranded (ds) forms, steric protection of adsorbed nucleotides from attack by nuclease enzymes, and DNA intercalation by GFNs of small lateral dimension. These unique modes of interaction open up a variety of application opportunities as well as potential safety concerns.

Lu *et al.* [47] report that an oligonucleotide molecular beacon (MB) adsorbs on GO and is released in the presence of complementary DNA, which implies that the single-stranded form adsorbs preferentially to the double stranded form. Lu *et al.* [47] also provide evidence for intracellular desorption in the presence of complementary RNA, and that the GO platform protects the DNA from enzymatic cleavage. It is argued that steric hindrance prevents nucleases from effectively attacking the adsorbed phase DNA. Similarly, Wang *et al.* [48] used small (100 nm) GO nanosheets as a fluorescent probe for intracellular ATP. An ATP aptamer conjugated with a dye was adsorbed on GO, which quenches the fluorescence until the atpamer forms a duplex with ATP, and desorbs to recover the fluorescence. Also, similar to Lu *et al.* [47], Wang *et al.* [48] report that GO protects the aptamer from enzymatic attack.

These two features: selective adsorption of ssDNA vs. dsDNA and the protection from degradative enzymes are making GO attractive in DNA or RNA delivery and sensing, especially when used in the form of < 100 nm “nanosheets” that have the advantages of dispersibility, colloidal stability, cell uptake, and low toxicity. We should note that the above studies follow the Sun *et al.* [38] technique of functionalizing the nano-GO with PEG, which is claimed to be necessary to achieve adequate stable dispersions in biological media. GO alone forms stable dispersions in water, but less stable dispersion in saline or media if not additionally functionalized.

Wu and coworkers [50] undertook a recent study to better understand the fundamentals of DNA adsorption on GO (Figure 4). Adsorption is found to be enhanced for small oligomers, and at low pH and high ionic strength, as might be expected by interaction of negative charges on DNA and GO. Also, ssDNA can be exchanged by free DNA in solution and can be effectively desorbed by complementary DNA in solution, but not effectively by increased temperature.

What is the fundamental reason for the preferential binding of ssDNA to GO relative to dsDNA? This trend was found empirically, but is now believed to reflect the role of GO-base interactions in ssDNA adsorption. DNA is a polyanion and is electrostatically repelled from GO, but the DNA bases can bind to graphenic surfaces through hydrophobic forces and π-π stacking [50]. These latter attractive forces can overcome the electrostatic repulsion, especially in the presence of high ionic strength where electrolytes shield the charges, or at low pH where GO charge is reduced by protonation. In dsDNA, the bases are protected inside the double helix and the outer charged phosphate groups show low affinity for GO surfaces.

A final example of strong GO/ssDNA interactions is the hydrogel synthesis of Xu *et al.* [49]. The authors do not study DNA adsorption per se, but rather mix dsDNA with GO and heat to 90 ° C causing uncoiling to ssDNA and conversion of the mixture to a stable hydrogel. The gelation is attributed to noncovalent ssDNA interactions with GO that bridge the individual sheets and XRD evidence is presented to support the physical bridging mechanism. At the level of a single GO sheet, this interaction is related to ssDNA adsorption and its selective adsorption relative to dsDNA. A different but related concept was pursued

NIH-PA Author Manuscript

NIH-PA Author Manuscript

NIH-PA Author Manuscript

by Sheng *et al.* [43] who used a GO platform in an aptamer-based sensing method for the model fungal food contaminant, ochratoxin A. The concept is to selectively bind the toxin with a fluorescently-tagged aptamer, and to use GO to adsorptively quench the unbound aptamer, but not the bound form, which adopts a antiparallel G-quadruplex confirmation that is less prone to adsorption on the planar surface of GO [43]. The authors find, however, that achratoxin adsorption on GO limits the sensitivity of the technique, and introduce PVP as a GO coating, which improves sensitivity. Here GO is used as a quenching agent, but its native surface chemistry is not selective enough in the adsorption of one aptamer confirmation over another.

A very different mode of DNA interaction is reported by Ren *et al.* [46], who provide evidence that nGO intercalates between base pairs in dsDNA, in a manner similar to planar aromatics that are known DNA intercalants. In the presence of Cu^{2+}, Ren *et al.* [46] report DNA cleavage, under conditions where Cu^{2+} alone is not active. It appears that the behavior relies on a combination of the planar single-atom-thick GO structure, which can be inserted in the molecular spaces between base pairs, and the peripheral COOH groups that provide sites for Cu^{2+} binding (Figure 5). These two features bring redox-active Cu^{2+} in direct proximity to vulnerable target sites in the DNA double helix and catalyze oxidative cleavage. This finding may lead to concern about potential toxicity of small-dimension GO in the human body, but may also open up applications for new chemotherapeutic agents in the common class that work through DNA intercalation.

4.3 Lipid and protein interactions

Relative to DNA and to small molecule drugs, there is little information on the interaction of GFNs with lipids or proteins. The two-dimensional geometry of GFMs may lead to unique interactions with lipid assemblies. Titov and coworkers [51] use coarse-grained molecular dynamics simulations to study the interaction of monolayer to few-layer graphene (up to 8 layers) with lipid bilayers. The GFMs are observed to localize in the hydrophobic core (Figure 6) with minimal perturbation of the overall bilayer thickness when layer number is small [51]. The work suggests the ability to form stable and functional graphene-lipid hybrid structures, though experimental data are lacking.

Other nanomaterials have been shown to interact with lipid molecules to change the fluid-gel phase behavior of bilayers [52, 53]. Electrostatic interaction with head groups can promote bilayer gelation (seen for negatively charged particles) or promote fluidity (seen for positively charged particles) [53]. The behavior of GFMs is unknown, but in comparison to nanoparticles of similar hydrodynamic size, GFMs have very large potential for lipid interaction due to their extended 2D surface.

Protein adsorption on nanomaterial surfaces is believed to mediate cell uptake and thus toxic responses, and has been receiving increasing attention over the last several years (reviewed by Nel et al. [23]). Due to high specific surface area, GFNs possess potentially larger protein adsorption capacities than most other nanomaterials. There have been few studies of GFN-protein or GFN-amino-acid interactions. Zhang *et al.* [54] use peptide adsorption on GO as the basis for a sensing technology targeted at protease activity. Fluorescently tagged peptides are first physically adsorbed on nGO, where they reside in a quenched state. Protease activity (here thrombin) cleaves the peptide, releasing the tagged tail to recover fluorescence. It is notable that GO protects ssDNA from nucleases [47] but does not protect (these) peptides from proteases, a difference which is not presently addressed in the literature, but may have to do with the geometries and confirmations of the adsorbed states and the enzyme active sites. Zhang *et al.* [54] support this study with fundamental measurements of single amino acid adsorption on nGO, and find that positively charged side chains, and aromatic side chains promote adsorption – the same trend reported for amino

NIH-PA Author Manuscript

NIH-PA Author Manuscript

NIH-PA Author Manuscript

acid adsorption on SWNTs [26]. Qin *et al.* [55] used density functional methods to study the adsorption of the amino acid L-leucine on graphene surfaces. More research is clearly needed on the interaction of proteins with graphene-family nanomaterials.

4.4 Oxidative reactions

Recently Liu *et al.* [56] studied the interaction of carbon nanomaterial surfaces with the antioxidant glutathione, and report catalytic activity for the glutathione-O_2 reaction for a range of materials including GO. The reaction is dependent on surface area and increases with structural disorder and nitrogen doping [56]. GO has significant catalytic activity for this model reaction, and may thus mediate oxidative damage in living systems, although it shares this property with other members of the carbon nanomaterial family such as nanotubes and carbon black. Chang *et al.* [57] report oxidative stress upon exposure of A549 cells to GO, but it is unclear whether this cellular endpoint reflects direct mediation of oxidation reactions on GO surfaces or indirect generation of cellular-derived oxidants following interaction with GO.

4.5 Biological Degradation

Resistance of carbon nanomaterials to biological degradation is a major factor responsible for biological durability or biopersistence in intact organisms, especially following inhalation into the lungs [58]. High aspect ratio nanomaterials such as carbon nanotubes share similar characteristics with asbestos fibers including size, high surface area and reactivity, and biopersistence that is a concern for potential lung toxicity [59]. In acellular assays, SWNTs are usually not degraded under conditions that simulate the phagolysosome of macrophages unless they are carboxylated [60]. Carboxylated SWNTs are also susceptible to biodegradation by exposure to hydrogen peroxide and horseradish peroxidase [61] or hypochlorite and the mammalian enzyme myeloperoxidase [62]. Kotchey *et al.* [63] also reported that GO, but not rGO, is susceptible to oxidative attack by hydrogen peroxide and horseradish peroxidase. This observation may enable design of safer GFNs [64] that are potentially biodegradable in order to minimize adverse environmental and human health impacts.

5. Potential for Human Exposure

There are four distinct entry routes for nanomaterials into the human body: inhalation, ingestion, dermal penetration, and injection or implantation for biomedical applications. For many materials, inhalation exposure often contributes the highest risk, and there is significant evidence that correlates inhaled ultrafine and ambient particles with adverse health effects [65–67]. To our knowledge, there have been no reports of or experimental studies on exposure to airborne GFNs. As discussed above, however, some GFNs are processed as dry powders, for which inhalation exposures must at least be regarded as a possibility. GFNs are unique powders, however, with plate-like structure, atomic thinness, and extreme aspect ratio. The implications of this unique geometry for inhalation exposure and deposition patterns are explored in the following section. Biomedical applications will be discussed in Section 7.

5.1 Deposition and Clearance in the Human Respiratory Tract

Mathematical models, such as the International Commission on Radiological Protection [68] and the National Council on Radiation Protection and Measurement [69], have been developed for predicting total and regional deposition of particles in the human respiratory tract [70]. These models predict the dose to organs and tissue due to inhalation of radioactive particles by men and women, both adults and children. Both models are based on experimental data, theory, and an earlier ICRP model developed in the 1960s. The models predict regional and

NIH-PA Author Manuscript

NIH-PA Author Manuscript

NIH-PA Author Manuscript

total deposition in the human respiratory tract for a wide range of aerosolized particle sizes and cover a full range of breathing conditions. Specifically, the ICRP model predicts deposition fractions using empirical equations based on experimental data and theory. It accounts for various deposition mechanisms such as settling, inertia, and diffusion in five regions of the respiratory system: the nose and mouth, throat and larynx, upper airways (bronchi), lower airways (bronchioles), and alveoli.

Inhaled particles may deposit in various regions of the respiratory tract by impaction, sedimentation, and diffusion or they may be exhaled. The retention time for particles depends on their site of deposition and interactions with the airway surface. If the particles deposit in the conducting airways, the retention time is short due to efficient mucociliary and cough clearance. The conducting airways consist of the nose, nasopharynx, larynx, trachea, bronchi and bronchioles [71]; the trachea, bronchi and bronchioles form the tracheobronchial region of the lung (generations 1–16 in the bifurcating airway model). The main function of the conducting airways is to act as a conduit for movement of air into the respiratory tract and to filter, warm, and humidify the incoming air. Mucociliary clearance is the predominant mechanism of particle clearance in the conducting airways. The rate of clearance depends on ciliary function and physical parameters of the respiratory tract lining fluids. As particles deposit more proximally, deeper into the lung, the retention time increases as a result of decreasing mucociliary clearance.

Mucus is produced in the airways by serous cells, goblet cells, and Clara cells and protects the airway epithelia from foreign substances. This secretion provides a renewable and mobile layer that can interact with, trap, and clear harmful substances. Mucus is a viscous solution that has defined physical and chemical properties that enable it to be transported out of the respiratory tract by ciliary motion of the ciliated cells that line the airways. Mucus glycoproteins or mucins are structural and secretory products of all secretory epithelia, including the airway epithelium [72–74]. Mucins that form the mucus gel resemble long flexible strings that are densely coated with short glycans some of which are negatively charged at their ends due to the presence of carboxyl or sulfate groups [75]. The glycosylated and hydrophilic regions are interspersed with hydrophobic domains of the protein that fold into hydrophobic globules stabilized by multiple internal disulfide bonds. Alternating regions of hydrophilic and hydrophobic domains is what imparts mucus its tenacity to trap particles with great efficiency. Each mucin fiber, as a result of its flexible array of alternating hydrophilic and hydrophobic domains, can conform to any surface of an “interacting” particle and form multiple low-affinity bonds. Respiratory cilia then clear the mucus blanket of pathogens and environmental debris from the upper and lower respiratory passages by beating in a coordinated and rhythmic manner [76].

Some inhalable particles have regular geometric shapes while others such as agglomerates or crushed materials have irregular shapes. The shape of a particle affects its drag force and settling velocity thus a correction factor, a shape factor, is applied to account for the effect of shape on particle motion. The dynamic shape factor is defined as the ratio of the actual aerodynamic resistance force of a nonspherical particle to the resistance force of a sphere having the same volume and velocity as the nonspherical particle. Some GFNs are atomically thin, and all GFNs have very high aspect ratios that deviate markedly from spherical or equi-axed particles.

To our knowledge there have been no studies of the aerodynamic behavior or respiratory deposition patterns of the extreme plate-like GFNs. We therefore set out to estimate their regional deposition in the respiratory tract using shape factors determined for oblate spheroids [77] as a function of layer number and lateral dimension. GFNs are anisotropic particles with a short (polar) and a long (equator) axis, and may move along the polar axis or

NIH-PA Author Manuscript

NIH-PA Author Manuscript

NIH-PA Author Manuscript

perpendicular to the polar axis. Equations (2) and (3) describe the shape factors for each transport mode. A ratio, q, is defined for short, a, and long, b, axes: q= a/b. Using this ratio, the shape factor for particles moving along the polar axis is:

$$\chi_{\parallel}=\frac{\frac{4}{3}(1-q^2)q^{-1/3}}{\left(\frac{1-2q^2}{\sqrt{1-q^2}}\right)\cos^{-1}q+q} \tag{2}$$

and for a particle moving perpendicular to the polar axis:

$$\chi_{\perp}=\frac{\frac{8}{3}(1-q^2)q^{-1/3}}{\left(\frac{3-2q^2}{\sqrt{1-q^2}}\right)\cos^{-1}q-q} \tag{3}$$

For nonspherical particles, as in the case of GFNs, the aerodynamic diameter is

$$d_a=d_e\left(\frac{\rho_p}{\rho_0\chi}\right)^{1/2} \tag{4}$$

where d_a is the aerodynamic diameter, d_e is the volume equivalent diameter, ρ_p is the density of the material, ρ_0 is the standard particle density and χ is the shape factor [70]. The following equations have been fitted to the ICRP model for monodisperse spheres of standard density at standard conditions but they can be applied to other particles by using the aerodynamic diameter for particles larger than 0.5 μm [70]. The inhalable fraction, *IF*, as used by the ICRP model is:

$$IF=1-0.5\left(1-\frac{1}{1+0.00076d_p^{2.8}}\right) \tag{5}$$

where d_p is the particle size in mm. The deposition fraction in the head airways region, DF_{HA}, is:

$$DF_{HA}=IF\left(\frac{1}{1+\exp(6.84+1.183lnd_p)}+\frac{1}{1+\exp(0.924-1.885lnd_p)}\right) \tag{6}$$

The deposition fraction in the tracheobronchial region, DF_{TB}, is:

$$DF_{TB}=\left(\frac{0.00352}{d_p}\right)[\exp(-0.234(lnd_p+3.40)^2)+63.9\exp(-0.819(lnd_p-1.61)^2)] \tag{7}$$

Whereas, the deposition fraction in the alveolar region, DF_{AL}, is:

$$DF_{AL}=\left(\frac{0.0155}{d_p}\right)[\exp(-0.416(lnd_p+2.84)^2)+19.11\exp(-0.482(lnd_p-1.362)^2)] \tag{8}$$

NIH-PA Author Manuscript

NIH-PA Author Manuscript

NIH-PA Author Manuscript

Using the above equations, the regional deposition for 3 GFNs of different lateral dimension has been calculated and shown in Figure 7.

As shown in Figure 7, there may be substantial deposition of all 3 sizes of GFNs throughout the respiratory tract. The deposition is higher for the smallest (0.5 μm) and largest (25 μm) of the three GFNs considered. Independent of the particle orientation, deposition efficiencies can be as high as 45 % for the 0.5 μm GFN in the alveolar region. Even GFNs as large as 25 μm can travel to the pulmonary region with reasonable efficiencies (10 %) due to transverse thinness. Figure 8 provides estimates for deposition of GFNs ranging from 5 nm to 100 μm in their lateral dimensions. Particle deposition in the alveolar region is as high as 50 % for GFNs with a lateral dimension of approximately 100 nm, irrespective of their orientation.

Figure 9 shows the aerodynamic diameters of GFNs as a function of lateral size and layer number. The aerodynamic diameters are always much less than the quoted lateral dimension due to the ultrathin nature of GFNs in the transverse direction, which also contributes to the calculation of aerodynamic size. The orientation of the particle as it travels through the fluid also becomes more important with increasing size as is evident from the separation in the two curves for particles 0.5 μm and larger (Figure 9D–F). Movement perpendicular to the layer planes gives high flow resistance and lead to smaller effective sizes, as expected. Similar particle aerodynamic diameter curves can also be generated for particles of intermediate lateral dimensions. Finally, we note that GFNs in the dry state, like other nanomaterials, have a strong tendency to aggregate into stacked plate structures, and in some cases may also fold or crumple during processing, and each of these behaviors will modify their effective shape and deposition patterns.

In general, is important that all three components of mucociliary clearance (epithelium, cilia, and mucus) must function properly for efficient clearance of GFNs and to protect the pulmonary region from potential toxic insult. The alveolar region does not have a protective mucus layer due to its gas exchange function. GFNs deposited in the alveolar region region may be engulfed by alveolar macrophages and cleared very slowly over months or years. The biopersistence of GFNs may impair this clearance mechanism and potentially cause scarring or fibrosis of the alveolar region. Further, hydrophobic materials may adhere strongly to mucins [78, 79] causing them to bundle together and increasing the pore size in the mucus mesh [80–84]. Thus, respiratory tract mucus is a critical diffusional barrier that may offer significant protection of the airways against GFNs. It is important to study the interactions between GFNs and respiratory tract lining fluids in order to understand natural protective defense mechanisms. Alternatively, hydrophobic GFNs that enlarge mucin pores may increase susceptibility to microbial penetration and infection [84].

5.2 Observed Behavior of Plate-Like Minerals

It is useful to consider our experience with other nonfibrous, plate-like materials. There have been occupational exposures to plate-like minerals in industries that mine and use talc, mica, slate, kaolin, and Fuller's earth. These minerals contain silicates, and some of these particles are respirable. Heavy exposure is known to result in accumulation in the respiratory bronchioles, in the interstitium surrounding the bronchioles and blood vessels, and in lymphatics and lymph nodes associated with the lungs [7]. Following chronic inhalation, these dust aggregates may become fibrotic with collagen deposition. This pattern of focal dust accumulation has also been described in graphite workers [85]. Inhalation of talc and other plate-like minerals can also induce granulomas in the lungs [86]. Granulomas are formed in response to biopersistent foreign materials that are not readily engulfed and degraded by macrophages. Granulomas are an aggregate of activated macrophages that frequently contain multinucleated giant cells formed by the fusion of macrophages that surround the

NIH-PA Author Manuscript

NIH-PA Author Manuscript

NIH-PA Author Manuscript

foreign material [87]. These lesions, as well as focal and interstitial fibrosis, are also induced by instillation or inhalation of carbon nanotubes in rodents [88].

In summary, there is the potential for substantial deposition of inhaled GFNs in the human respiratory tract, and the deposition will depend on lateral dimension, layer number, orientation in the airflow, and possibly stiffness. Based on experience with other materials, hydrophobic GFNs may increase microbial penetration into the mucus layer. In the alveolar regions, deposited GFNs may impair clearance, form granulomas, and possibly produce fibrosis similar to carbon nanotubes [88]. The major discussion of adverse responses to GFNs appears in the next section.

6. Toxicity and Biocompatibility

Similar to other carbon nanomaterials, GFNs may elicit adverse responses from prokaryotic or bacterial cells as well as eukaryotic mammalian cells. In contrast to carbon black nanoparticles or carbon nanotubes, much less is known about interactions with target cells and potential toxicity of GFNs. GFNs may be inhaled into the lungs (Section 5), deliberately injected intravenously for drug delivery, or implanted for tissue engineering (Section 7). This section will review potential toxicity of GFNs for bacteria, mammalian cells in the lungs, and other mammalian target cells following intravenous injection or implantation. Systemic distribution and potential acute and chronic effects will also be considered.

6.1 Bacterial toxicity

A number of studies report bacterial toxicity of GFNs and suggest they may find future application in antimicrobial products. Kang *et al.* showed that highly purified CNTs inactivated *E. coli* [89,90]. Akhavan *et al.* [91] investigated the bacterial toxicity of GO and reduced graphene against Gram-negative, *E. coli*, and Gram-positive, *S. aureus* bacteria. Both GO and rGO were effective as antibacterial materials with rGO exhibiting the strongest antibacterial effectiveness. Similar results were obtained by Hu *et al.* [92] where they investigated the antibacterial activity of both GO and rGO on *E. coli*. Within 2 hours, *E. coli* cell metabolic activity was reduced to approximately 70 % and 13 % at concentrations of 20 and 85 mg/ml respectively. The authors confirmed these results using transmission electron microscopy [93], which revealed that the bacterial cells lost membrane integrity. These experiments suggest that GO and rGO produce bacterial membrane damage upon contact, although the fundamental toxicity mechanism and its relationship to specific GFM material properties awaits further study.

In contrast to these studies, the *Shewanella* family of bacteria are capable of metal reduction and have been shown to reduce GO in suspension cultures with no inhibition of bacterial growth. [94] Microbial reduction of GO provides a unique, nontoxic approach for synthesis of graphene.

Intercalation of redox active metal ions such as Fe^{2+} between GO sheets (described in Section 4.2) may also be exploited for bacterial killing. Natural nanoscale clays containing adsorbed metals have been shown to kill bacteria. This antibacterial activity does not require direct physical contact but depends on aqueous leaching of Fe^{2+}, intracellular transport, and generation of hydroxyl radicals intracellularly resulting in bacterial death [95]. This mechanism could be exploited by designing metal-intercalated GO sheets for external application to treat wounds infected with antibiotic-resistant bacteria.

6.2 Mammalian Cell Toxicity *in vitro*

Potential target cells in the lungs following inhalation of GFNs include alveolar macrophages, lung epithelial cells, and fibroblasts in the interstitium of the alveolar walls [88].

NIH-PA Author Manuscript

NIH-PA Author Manuscript

NIH-PA Author Manuscript

Macrophages are the initial cell that responds to inhaled microorganisms or particulates [96]. Although there is the potential for human inhalation exposure to GFNs, to our knowledge there are no published papers using macrophages as target cells. We used the human monocytic cell line, THP-1, to investigate initial interactions with FLG of different lateral dimensions. As illustrated in Figure 10, these cells readily internalize carbon black nanoparticles, carbon nanotubes, and FLG up to 5 μm in lateral dimension. When exposed to 25 μm FLG, the cells adhere to the surface initially and gradually spread to surround and cover the surface of these large FLG sheets (Figure 11). Exposure of macrophages to CNTs induces macrophage activation and granuloma formation [97]; it is unknown whether GFNs will also induce similar responses.

The interaction between dispersed graphene or GO sheets and target cells has been studied in monolayer cultures of lung epithelial cells [57], fibroblasts [98] and neuronal cells [99]. Single-layer GO sheets were internalized and sequestered in cytoplasmic, membrane-bound vacuoles by human lung epithelial cells or fibroblasts and induced toxicity at doses above 20 μg/ml after 24 hours [98, 100]. Chang *et al.* [57] using human lung epithelial cells found minimal toxicity at doses higher then 50 μg/ml and no cellular uptake. However, they did demonstrate extracellular generation of ROS. Zhang *et al.* [99] also reported that few-layer graphene increased intracellular generation of ROS and induced mitochondrial injury in neuronal cells after 4 and 24 hours at a dose of 10 μg/ml. Surface modification of graphene has been reported to alter its toxicity [47] with reduced GO and carboxylated graphene reported to be less toxic than GO or native graphene [101]. Fetal bovine serum in the cell culture medium has also been reported to decrease toxicity using A549 human lung epithelial cells [100]. No information is given on lateral size or dispersion behavior.

Direct or indirect generation of reactive oxygen species leading to oxidative stress in target cells is the leading mechanism proposed for toxicity of engineered nanomaterials [102, 103]. Normal cellular homeostasis is a balance between the level of ROS generation and its elimination or reduction by antioxidant enzymes. Levels of ROS are balanced by action of superoxide dismutase (SOD), catalase, or glutathione (GSH) peroxidase; when levels of ROS cannot be reduced by cellular antioxidant activity, this may lead to alteration of macromolecules such as polyunsaturated fatty acids in membrane lipids, protein denaturation, and ultimately DNA. Little is known about toxicity pathways for GFNs. Their chemical similarity to carbon nanotubes, however, as well as early studies on GFNs themselves [56, 57, 99] suggest that oxidative stress may be an important pathway in the graphene family.

Two-dimensional graphene nanomaterials are unique in comparison with spherical nanoparticles or one-dimensional nanotubes or nanorods, and the chemical and physical determinants for their cellular interactions and biocompatibility are unknown. We emphasize the need for systematic studies that address the role of layer number, lateral size, hydrophobicity, stiffness, and surface reactivity in determining adverse environmental and health impacts.

6.3 *In vivo* biodistribution and toxicity

GFNs with nanoscale dimensions and specific chemical modifications are being developed for intravenous drug delivery. Drugs and targeting molecules can be covalently attached to the graphene surface and edge site or polymers may be adsorbed onto the grapheme surface to enhance solubility [64]. PEG-coated nanographene sheets (10–50 nm) were fluorescently labeled and the biodistribution assessed in mice bearing tumor xenografts. The nanographene sheets accumulated in tumors with lower uptake by the reticuloendothelial system (RES) after 24 hours and no short-term toxicity [104]. A second study used nanographene sheets with PEG and labeled with radioactive iodine to assess biodistribution

NIH-PA Author Manuscript

NIH-PA Author Manuscript

NIH-PA Author Manuscript

and excretion following intravenous injection. These nanographene sheets accumulated initially in the RES, liver and spleen followed by gradual clearance after 3–15 days. After 3 months, the nanographene sheets were cleared and induced no toxicity at a dose of 20 mg/kg [105].

In comparison, two studies reported biodistribution and toxicity of graphene oxides following intravenous injection in mice. At doses of 0.1 or 0.25 mg, no toxicity was observed; however, a dose of 0.4 mg induced granulomas in the lungs, liver, spleen, and kidney and was lethal in 4/9 of the mice [98]. Zhang *et al.* [106] also noted deposition and retention in the lungs with production of lung injury, inflammation, and granuloma formation when delivered intravenously at a dose of 0.4 mg. Granulomas are also induced in the lungs of drug abusers following intravenous injection of drugs containing talc particles [86]. In summary, GFNs designed for intravenous drug delivery have the potential for bioaccumulation and granuloma formation although these potential complications may be decreased by surface modifications to achieve selective tumor targeting and to promote biodegradation following drug delivery as discussed in Section 4.5 and in Kotchey *et al.* [63].

6.4 Potential for foreign body tumorigenesis

Future biomedical applications of graphene-family materials may include implantable sensors, tissue scaffolds, or coatings on prosthetics or implanted devices. Nonbiodegradable foreign materials have induced sarcomas in rodents following implantation at a variety of anatomic locations (reviewed in IARC) [107]. This phenomenon is called solid state or foreign body carcinogenesis and it is hypothesized to be induced by biopersistent, smooth, continuous surfaces regardless of chemical composition [108–110]. Foreign body tumors are classified as sarcomas with a range of differentiation including muscle, blood vessels, connective tissue, and bone and are postulated to originate from a local mesenchymal stem or progenitor cell population [111]. Rare cases of human foreign body sarcomas have been reported in association with silicone breast implants, vascular grafts, and orthopedic implants (reviewed in IARC) [107].

It is unknown whether graphene-family materials have the potential to induce foreign body sarcomas. The biomaterial properties associated with foreign body sarcomas, however, include large size or surface area, smooth continuous surface, and biopersistence [112]. Rough surfaces, powdered materials, nonmetallic particulates, and porous materials (> 0.02 μm in diameter) are less likely to induce tumors [107]. Graphene-family materials can have very high surface areas, smooth topography, and may be biopersistent [113] similar to tumorigenic solid-state implants, hence the inclusion of this topic in the present review.

The temporal sequence of host responses to foreign bodies and medical implants has been studied in rodents (Figure 12) [114, 115]. Host-derived proteins including albumin, fibrinogen, and extracellular matrix components (fibronection, vitronectin) initially adsorb onto the surface of the implant followed by an early acute inflammatory response. Macrophages may fuse to form multinucleated giant cells on the implant surface, which is surrounded by a wound healing response characterized by ingrowth of new capillaries, fibroblast proliferation, and collagen deposition. After approximately three months, an acellular, dense fibrous collagen capsule surrounds the implant, which remains in a dormant phase [114]. After 8 months, proliferating cells appear in direct contact with the implant and may have an atypical appearance; this is defined as the preneoplastic phase [115]. Foreign body sarcomas have a very long latent period developing 26–110 weeks after implantation in rodents [115]. This long latent period may explain the rarity of foreign body sarcomas in humans who usually receive medical implants later in life [107].

NIH-PA Author Manuscript

NIH-PA Author Manuscript

NIH-PA Author Manuscript

In contrast to solid surfaces, porous cellulose acetate filters induce persistent inflammation characterized by multinucleated giant cells that infiltrate into the pores and surrounded the implant with minimal fibrosis [116]. Implantation of gelatin sponges induces an initial acute inflammatory response that resolves after one month as the gelatin is broken down [112].

Several mechanisms have been considered for foreign body tumorigenesis. Direct physical contact between progenitor or preneoplastic cells with the surface of a smooth, contiguous, biopersistent implant has been hypothesized as essential for carcinogenicity [108]. It is unlikely that additives, chemicals, or metal ions that leach slowly from medical implants contribute to carcinogenicity because inert biomaterials such as aluminum oxide ceramic and stable polymers including polytetrafluoroethylene produce foreign body sarcomas [107]. Kirkpatrick *et al.* [115] tested nine medical grade biomaterials implanted subcutaneously in rats as smooth disks and all of these materials which included one ceramic material, three metals, and five polymers induced sarcomas. Formation of a dense fibrous capsule surrounding the implant has been hypothesized to impair cell-cell communication allowing uncontrolled cell proliferation and aberrant cell differentiation that progress to tumor formation [116]. Finally, persistent inflammation accompanied by release of reactive oxygen and nitrogen species from infiltrating inflammatory cells has been hypothesized to promote DNA damage, epigenetic alterations, and tumor progression [117, 118]. Tazawa *et al.* [93] demonstrated local expression of inducible nitric oxide synthase and markers of oxidative and nitrative DNA damage in inflammatory and stromal cells 14 days after subcutaneous implantation of plastic films in mice [93]. Okada [112] hypothesizes that reactive oxygen and nitrogen species, inflammatory mediators, and growth factors released from inflammatory cells contribute to development of foreign body tumors. However, release of oxidants such as H_2O_2 or enzymes such as myeloperoxidase from inflammatory cells may also contribute to biodegradation of GFNs, as reported recently for some carbon nanotubes and for GO, [60, 62, 63, 119] and discussed earlier in this review.

The physicochemical properties of biomaterials responsible for induction of foreign body sarcomas are well-known, and in principle, it should be possible to engineer biomedical GFNs to prevent this adverse reaction. For example, the surface texture of graphene coatings can be altered through controlled folding or rippling to reduce smoothness and prevent inflammation [120] and formation of a thick fibrous capsule. Graphene could be employed in patches to reduce the extended surface, or selective surface functionalization may be exploited to create a biocompatible surface that will not elicit prolonged inflammatory and fibrotic responses.

7. Biomedical Applications

The limited early literature on GFNs suggests their potential as biosensors [14], tissue scaffolds [121, 122], carriers for drug delivery [38] or gene therapy [123], antibacterial agents [92], and bioimaging probes [10, 12, 38]. In biomedical applications, the major advantage of GFNs over other nanomaterials is their high specific surface area, which allows high-density biofunctionalization or drug loading. Due to their 2D structure, both sides of a single graphene sheet can be used as a substrate for the controlled addition or adsorption of molecules and functional groups. Both covalent and non-covalent surface modification has been used to impart specific biological activity to GFNs as well as to improve biocompatibility and colloidal stability. The most common covalent modifications include oxidation by Hummers method to make GO or rGO, conjugation of hydrophilic polymers, 1,3-dipolar cycloaddition, arylation, or amine coupling to carboxylic groups, while non-covalent modifications are often achieved using hydrophobic forces or π-π interactions on the pristine graphene surface or unmodified graphenic patches lying between functional groups on GO surfaces.

NIH-PA Author Manuscript

NIH-PA Author Manuscript

NIH-PA Author Manuscript

7.1 Drug delivery

Covalent attachment of chitosan [124], folic acid [10,125] and polyethylene glycol (PEG) [38, 126] to GO has been shown to produce a potential platform for the delivery of anti-inflammatory [124] and water-insoluble anticancer drugs such as doxorubicin (Dox) [10, 38, 125, 127], and SN38, a camptothecin analogue [126]. Functionalized in this way, nano-GO becomes dispersible and highly stable in physiological solutions such as cell culture media, serum, and phosphate buffered solution (PBS) and has been reported to show negligible or no toxicity *in vivo* [104, 105] and *in vitro* [38, 124, 126] at the doses used. Controlled loading of hydrophobic drugs onto GO by physisorption increases the total concentration of these compounds in the physiological suspension and aids in delivery. In many cases the driving force for physisorption is cited as π-π interaction and hydrophobic forces. For certain drug molecules, lowered pH increases their solubility and thus decreases their tendency to stay adsorbed, leading to potential controlled release in acidic lysosomes following cellular endocytosis [38, 40, 125, 127]. Relatively hydrophilic molecules are retained by GO-composites less than hydrophobic molecules in both physiological and acidic pH solutions [124].

Several approaches to drug delivery have been evaluated *in vivo* and *in vitro*. Rituxan [128], a monoclonal antibody against the B-cell membrane surface marker CD20, is often used in combination with chemotherapy drugs for the treatment of non-Hodgkin's lymphoma [129]. A composite made by covalent attachment of Rituxan to PEG-nano-GO together with physisorption of doxorubicin (Rit-PEG-nano-GO/Dox) was evaluated *in vitro* for targeting of Raji B-cells, a human Burkitt's lymphoma cell line. Rit-PEG-nano-GO/Dox improved cell growth inhibition when compared to free Dox, PEG-NGO/Dox, or PEG-NGO plus free Dox with or without free Rituxan [38]. In other study, SN38, a water insoluble topoisomerase I inhibitor produced by hydrolysis of the synthetic camptothecin (CPT), was adsorbed to PEG-nano-GO. CPT is used for colon cancer treatment and due to its high excretion rate only a part of the administrated dose is converted to SN38, its active form [130]. PEG-nano-GO/SN38 complexes are soluble and stable in water, PBS and serum with negligible or low release. *In vitro* testing showed that PEG-nano-GO/SN38 is equally effective to free SN38 in DMSO but approximately 1000 times more potent when compared to CPT in inducing death in HCT-116 cells, a human colon cancer cell line [126]. Simultaneous physisorption of Dox and CPT to GO previously covalently functionalized with both sulfonate groups (SO_3^-) to increase stability and folic acid (FA) for specific targeting of cancer cells expressing FA-receptor has been evaluated *in vitro* as well [10]. By using MCF-7 cells, a human breast cancer cell line expressing FA receptors, and A549 cells, a human adenocarcinomic alveolar basal epithelial cell line that do not express FA receptors, the authors shown specific uptake of FA-GO by MCF-7 cells. When treated with FA-GO/Dox/CPT, breast cancer cells were more sensitive compared to FA-GO/Dox or FA-GO/CPT.

FA-GO has been evaluated *in vitro* as a carrier for the photosensitizer chlorin e6 (Ce6). Photosensitizers are porphyrin-based molecules used in photodynamic therapy to induce cell death via generation of ROS upon irradiation [131]. Significant reduction in cell viability was reported in MGC803 cells, a human stomach cancer cell line positive for FA receptors, when exposed to FA-GO/Ce6 following irradiation with the appropriated wavelength [41].

Recently, it has been suggested that nanoscale PEG-GO can be a good candidate for photothermal cancer therapy due to its strong near-infrared [24] optical absorption. After 24 hrs of intravenous injection, PEG-nano-GO can passively accumulate in tumors of different xenograft tumor mouse models [104]. Upon irradiation at 808 nm with power density of 2 W/cm^2, a significant increased in tumor temperature is achieved leading to efficient tumor ablation. Although PEG-nano-GO accumulates in the reticuloendothelial system (RES) after intravenous administration, after 90 days post exposure, there was no indication of any toxicological or pathological effects. [104, 105]

NIH-PA Author Manuscript

NIH-PA Author Manuscript

NIH-PA Author Manuscript

7.2 Tissue engineering

The mechanical properties of graphene such as high elasticity, flexibility and adaptability to flat or irregular surfaces [132–134] are suitable for the structural reinforcement of biocompatible films, hydrogels and other scaffold materials frequently used for tissue engineering. Due to their resemblance to soft tissue, hydrogel composites have been extensively studied as scaffolds or cell-encapsulating fillers to generate or repair tissues such as skin, bladder, cartilage, and bone [135]. In general, compared to single-component hydrogels, composites present higher mechanical strength, stability, lubricity, water retention, and improved cell adhesion, differentiation and function [135–137].

Hydrogel composites made of synthetic hydrophilic polymers as polyvinyl alcohol (PVA) and poly(methyl methacrylate) (PMMA) have the potential to be used as fillers to repair cartilages, tendons and meniscuses, but have low mechanical strength or elasticity [135]. Incorporation of GO to PVA suspensions (GO/PVA) increases both the tensile strength and elasticity modulus of PVA hydrogels or films [138, 139] without affecting their potential for osteoblast attachment [139]. Similar results were obtained for films when GO was incorporated to PMMA [140], acid-functionalized FLG added to PVA or amide-functionalized FLG to PMMA [141]. In all cases, the increase of tensile strength and elasticity modulus was dependent on the concentration of graphene.

Chitosan gels are known to be osteoconductive and enhance bone formation [142]. Chitosan is a biocompatible and biodegradable polycationic biopolymer, generally obtained by alkaline deacetylation of chitin, the main component of the exoskeleton of arthropods. Structurally, it is similar to glycosaminoglycans, the major component of the extracellular matrix of bone. It can be gelled alone or as composites to be used as biological adhesive, and to promote wound-healing, and cellular attachment and proliferation [135, 142, 143]. Graphene can be used to reinforce chitosan films (GS/Cht) to improve their mechanical properties. Although GS/Cht films were not toxic when used as a substrate for culture of L929 cells, a murine fibrosarcoma cell line, they induce morphological changes dependent on the graphene concentration [144]. GO-chitosan scaffolds synthesized by covalent linkage of the carboxyl groups of GO with the amide groups of chitosan present a possible solution to control the rate of scaffold degradation used for hard tissue regeneration. GO-chitosan hydrogels retain their size and shape under physiological and extreme pH conditions, hold moisture longer, have lower degradation rate, and better mechanical strength when compared to chitosan alone. Moreover, they significantly improve cellular adhesion, proliferation, differentiation, and calcium and phosphate deposition of MC3T3-E1 cells, a mouse pre-osteoblast cell line [145].

Improvement of the osteogenic potential by graphene-coated surfaces with different stiffness and roughness has been reported by *in vitro* evaluation of differentiation of human mesenchymal stem cells (hMSCs) and pre-osteoblasts into osteoblasts [121, 122]. Polydimethylsiloxane (PDMS), poly- ethylene terephthalate (PET), glass, and Si/SiO_2 substrates, with or without coating, support stem cell-like morphology, cellular viability and proliferation when hMSCs are cultured using normal stem-cell medium. Compared to uncoated surfaces, when cultured in osteogenic medium without the addition of growth factors, hMSCs show increased expression of specific osteoblast cellular markers and calcium deposition on graphene-coated surfaces, independent of the stiffness of the substrate. Moreover, the differentiation rate induced graphene-coated surfaces was similar to the rate induced by the addition of BMP-2 to osteogenic medium in uncoated surfaces [121].

Another promising approach to be used for fabrication of graphene-based scaffolds is protein micropatterning. Using a PDMS stamp for microcontact printing, spatial patterning of laminin onto micro-scale epitaxial graphene has been achieved with micrometer-

NIH-PA Author Manuscript

NIH-PA Author Manuscript

NIH-PA Author Manuscript

resolution [146]. Irreversible physisorption by π-stacking of bifunctional 1-pyrenebutanoic acid succinimidyl ester via its aromatic pyrenyl group to graphene leaves a free succinimidyl ester group. Subsequently, covalent attachment of lamin occurs via nucleophilic substitution of N-hydroxysuccinimide by the amine residue of lysines, resulting in the formation of an amide bond [146, 147].

7.3 Other biological and medical applications

The literature contains a variety of other studies in which GFNs intersect the world of biology or medicine. For example, graphene has been proposed as a substrate for biomolecular imaging by TEM [148]; as a component in electrodes for neural stimulation [149], and as a platform for introducing nanopores used for DNA sequencing [150]. Bacteria have been reported to reduce GO [151], and phage display has been used to functionalize GFNs [152].

A major area for GFNs is their development is molecular probes that use fluorescence or fluorescence quenching. Due to its stability and biocompatibility, PEG-GO has been evaluated as platform for covalent attachment of fluorophores for *in vivo* and *in vitro* cellular imaging. Cy7, a NIR fluorescent dye, was covalently conjugated to six-branched PEG-GO via the formation of an amide bond (Cy7-PEG-GO). Whole-body fluorescence imaging show that after 24 hrs of intravenous administration into mouse models with different xenograft tumors, Cy7-PEG-GO passively accumulates into tumors [104]. Labeling of HeLa cells, a human cervical cancer cell line, using fluoresin (excitation 495 nm/emission 521 nm) covalently attached to PEG-GO (F-PEG-GO) has been reported. Instead of six-branched PEG, a linear PEG polymer was used as a bridge to covalently attach the aromatic fluorophore, preventing physisorption and quenching of the fluorophoro by GO. Cellular internalization of F-PEG-GO is suggested to occur by an energy-independent mechanism [153].

Molecular beacons (MBs) probes have been used, among other applications, to detect specific mRNA expression in living cells. MBs are small self-complementary hairpin-shaped DNA sequences, with close proximity terminal-labeled ends, bringing together a fluorophore and a quencher. Upon hybridization with its complementary target, the opening of the stem restores the fluorescence [154]. Adsorption of MB to nano-GO can be used as an alternative strategy for the cellular delivery MB with high efficiency and to prevent DNA digestion before MB interacts with its target. Upon cellular exposure, internalization of MB/GO leads to detectable expression of mRNA in HeLa cells [47]. These are intended as examples rather than an exhaustive coverage of GFN-based probes.

8. Conclusions and Research Needs

The literature on graphene family nanomaterials (GFNs) in biology is growing rapidly, although it remains a small subset of the total literature on these new 2D materials. Similar to carbon nanotubes, graphene forms a material *family* with variation in layer number, lateral dimension, and surface chemistry, and these variations are likely to influence the biological response. GFNs show several unique modes of interaction with biomolecules including preferential adsorption of single-stranded over double-stranded DNA, interleaflet insertion in the hydrophobic core of lipid bilayers, DNA intercalation in the presence of copper cations, and high cargo-carrying capacity for conjugated small molecule drugs, which can be physically adsorbed and reversibly desorbed. This set of unique biomolecular interactions make the graphene-bio interface an exciting area for further scientific study. A number of biomedical applications have been proposed for GFNs, with the largest set of studies focusing on nano-GO in drug delivery and fluorescence-based biomolecular sensing.

NIH-PA Author Manuscript

NIH-PA Author Manuscript

NIH-PA Author Manuscript

There is also an emerging literature on potential health risks. Despite the popular image of graphene as a large-area substrate coating, many graphene-family materials are dry powders at some point in their processing, and in this form pose the most significant exposure risk through inhalation. Of particular concern are few-layer graphene samples directly following the thermal exfoliation step or after washing and drying. There is need for measurement of airborne dust levels in research laboratories, and in pilot and full-scale manufacturing facilities. Aerodynamic diameters and deposition profiles have been estimated here from published theories on thin plate hydrodynamics. These calculations indicate the potential for significant deposition, but the extreme aspect ratios of graphene lead to some uncertaintly in shape factor, especially for the smaller materials, and experimental work is needed to confirm the predicted behaviors. GFNs that are made by wet chemical techniques and used in suspension are less likely to produce human exposures, though there is concern about spray processes (e.g. for GO-based coatings), or during sonication in open containers.

In the area of toxicity, there have been a number of studies reported, but the field is too young and the literature too limited to reach conclusions about potential hazards sufficient for risk assessment or regulation. Nano-GO has been reported to be biocompatible in a number of the studies focused on biomedical applications, at least under the limited conditions covered by such studies. Other studies have reported adverse biological responses, including cytotoxicity using human lung epithelial cells and fibroblasts [48, 92].

Cellular uptake of GFNs has been shown for macrophages (Figure 10) and human lung epithelial cells in some studies [100], although there have been no studies exploring the mechanism of uptake and intracellular fate. These sheet-like GFNs may physically perturb cytoskeletal organization, mitosis, organelle integrity, and impair cell motility and secretion. A potential toxicity pathway for GFNs is oxidative stress [57, 99] although it is not clear whether oxidant generation is related to reactive edge sites or an indirect response of target cells to nanomaterials. It is clear that lateral size is a key variable in cell uptake, while layer number affects deposition and surface area, and surface chemistry has a large affect on adsorption and dispersibility. Molecular dyanamics modeling of interactions between GFNs and cell membranes should provide valuable information about uptake mechanisms. Systematic investigation of toxicological endpoints using a defined set of carbon nanomaterials including carbon black, carbon nanotubes, and GFNs will be important to develop structure-activity relations (SARs).

Cellular assays using target cells in the lungs, especially macrophages, epithelial cells, and fibroblasts, are needed to assess potential of GFNs to cause acute toxicity, inflammation, and fibrosis following inhalation relative to other carbon nanomaterials such as carbon black and carbon nanotubes. Interactions of GFNs with mucus barriers in the respiratory and gastrointestinal tracts, as well as lung lining fluid in the aveoli, must be assessed, in addition to the potential of GFNs to overwhelm macrophage-mediated defenses and clearance. *In vivo* animal studies are also needed to assess biodistribution, biopersistence and chronic toxicity including induction of foreign body tumors, following inhalation, injection, or implantation.

Because graphenes form a material family with wide variation in properties, the graphene-bio field will benefit greatly in the long run, if its authors show diligence in characterizing their materials, and describing them according to layer number, lateral size, surface chemistry rather than *ad hoc* sample names. We propose a systematic nomenclature in this article that may be helpful in this regard. The nomenclature involves a limited number of GFN types: monolayer graphene, few-layer graphene (FLG), graphene oxide (GO), and reduced graphene oxide (rGO), along with the modifying prefix “nano” which can be applied to any of the materials to denote lateral dimensions below 100 nm. The names do

NIH-PA Author Manuscript

NIH-PA Author Manuscript

NIH-PA Author Manuscript

not fully define the material, but could provide convenient labels with which to refer to them in rationally defined categories. As a final note, GFNs are high-surface-area materials with corresponding high potential to cause adsorptive and quenching artifacts in biological assays. More work is needed in this area, and authors must be skeptical of standard assays without extensive controls for possible interference by GFNs.

Acknowledgments

Funding Support

Financial support for this work was provided by the NIEHS Superfund Research Program P42 ES013660, NIEHS T32 ES007272 Training Grant, NIEHS R01 ES016178 Grant and NSF CBET-1132446 (Barbara Karn, project manager). Though supported in part by the NIEHS the work does not necessarily reflect the views of the agency.

We thank Paula Weston in the Molecular Pathology Core Facility and Megan A. Creighton for their assistance with microscopy. The authors would like to acknowledge Cabot Corporation (Boston, MA) for compiling and providing industrial samples of few-layer graphene materials.

Abbreviations

AFM	atomic force microscopy
BET	Brunauer, Emmet, and Teller
BMP-2	bone morphogenetic protein-2
Ce6	chlorin e6
CNTs	carbon nanotubes
CPT	camptothecin
DMSO	dimethyl sulfoxide
Dox	doxorubicin
ds	double-stranded
EHS	environmental health and safety
FA	folic acid
FLG	few-layer graphene
GFNs	graphene-family nanomaterials
GNS	graphene nanosheets
GO	graphene oxide
hMSCs	human mesenchymal stem cells
MB	molecular beacon
Nano-GO	graphene oxide with nanoscale lateral dimension
PDMS	polydimethylsiloxane
PEG	polyethylene glycol
PMMA	poly(methyl methacrylate)
PVA	polyvinyl alcohol
PVP	polyvinylpyrrolidone
RES	reticuloendothelial system

NIH-PA Author Manuscript

NIH-PA Author Manuscript

NIH-PA Author Manuscript

rGO	reduced graphene oxide
Rit	Rituxan
ROS	reactive oxygen species
SAR	structure activity relation
SEM	scanning electron microscopy
SOD	superoxide dismutase
ss	single-stranded
SWNT	single-walled carbon nanotube
TEM	transmission electron microscopy
XRD	X-ray diffraction

References

1. Novoselov KS, Geim AK, Morozov SV, Jiang D, Zhang Y, Dubonos SV, Grigorieva IV, Firsov AA. Electric field effect in atomically thin carbon films. Science. 2004; 306:666–669. [PubMed: 15499015]
2. Ruoff R. Graphene: calling all chemists. Nat Nanotechnol. 2008; 3:10–11. [PubMed: 18654440]
3. Stankovich S, Dikin DA, Dommett GH, Kohlhaas KM, Zimney EJ, Stach EA, Piner RD, Nguyen ST, Ruoff RS. Graphene-based composite materials. Nature. 2006; 442:282–286. [PubMed: 16855586]
4. Su FY, You C, He YB, Lv W, Cui W, Jin F, Li B, Yang QH, Kang F. Flexible and planar graphene conductive additives for lithium-ion batteries. J Mater Chem. 2010; 20:9644–9650.
5. Paek SM, Yoo E, Honma I. Enhanced cyclic performance and lithium storage capacity of SnO2/graphene nanoporous electrodes with three-dimensionally delaminated flexible structure. Nano Lett. 2009; 9:72–75. [PubMed: 19090687]
6. Dikin DA, Stankovich S, Zimney EJ, Piner RD, Dommett GH, Evmenenko G, Nguyen ST, Ruoff RS. Preparation and characterization of graphene oxide paper. Nature. 2007; 448:457–460. [PubMed: 17653188]
7. Bunch JS, Verbridge SS, Alden JS, van der Zande AM, Parpia JM, Craighead HG, McEuen PL. Impermeable atomic membranes from graphene sheets. Nano Lett. 2008; 8:2458–2462. [PubMed: 18630972]
8. Compton OC, Kim S, Pierre C, Torkelson JM, Nguyen ST. Crumpled graphene nanosheets as highly effective barrier property enhancers. Adv Mater. 2010; 22:4759–4763. [PubMed: 20830709]
9. Wang S, Ang PK, Wang Z, Tang AL, Thong JT, Loh KP. High mobility, printable, and solution-processed graphene electronics. Nano Lett. 2010; 10:92–98. [PubMed: 20025234]
10. Zhang L, Xia J, Zhao Q, Liu L, Zhang Z. Functional graphene oxide as a nanocarrier for controlled loading and targeted delivery of mixed anticancer drugs. Small. 2010; 6:537–544. [PubMed: 20033930]
11. Ryoo SR, Kim YK, Kim MH, Min DH. Behaviors of NIH-3T3 fibroblasts on graphene/carbon nanotubes: proliferation, focal adhesion, and gene transfection studies. ACS Nano. 2010; 4:6587–6598. [PubMed: 20979372]
12. Feng L, Liu Z. Graphene in biomedicine: opportunities and challenges. Nanomedicine (Lond). 2011; 6:317–324. [PubMed: 21385134]
13. Shao Y, Wang J, Wu H, Liu J, Aksay IA, Lin Y. Graphene Based Electrochemical Sensors and Biosensors: A Review. Electroanalysis. 2010; 22:1027–1036.
14. Kuila T, Bose S, Khanra P, Mishra AK, Kim NH, Lee JH. Recent advances in graphene-based biosensors. Biosens Bioelectron. 2011; 26:4637–4648. [PubMed: 21683572]
15. Geim AK. Graphene: status and prospects. Science. 2009; 324:1530–1534. [PubMed: 19541989]

NIH-PA Author Manuscript

NIH-PA Author Manuscript

NIH-PA Author Manuscript

16. Sprinkle M, Ruan M, Hu Y, Hankinson J, Rubio-Roy M, Zhang B, Wu X, Berger C, de Heer WA. Scalable templated growth of graphene nanoribbons on SiC. Nat Nanotechnol. 2010; 5:727–731. [PubMed: 20890273]

17. Lotya M, King PJ, Khan U, De S, Coleman JN. High-concentration, surfactant-stabilized graphene dispersions. ACS Nano. 2010; 4:3155–3162. [PubMed: 20455583]

18. Park S, An J, Jung I, Piner RD, An SJ, Li X, Velamakanni A, Ruoff RS. Colloidal suspensions of highly reduced graphene oxide in a wide variety of organic solvents. Nano Lett. 2009; 9:1593–1597. [PubMed: 19265429]

19. Cote L, Kim J, Tung C, Luo J, Kim F, Jiaxing Huang J. Graphene oxide as surfactant sheets. Pure Appl Chem. 2011; 83:95–110.

20. Kim F, Cote LJ, Huang J. Graphene oxide: surface activity and two-dimensional assembly. Adv Mater. 2010; 22:1954–1958. [PubMed: 20432227]

21. Guo, F.; Kim, F.; Han, TH.; Shenoy, V.; Huang, J.; Hurt, RH. Hydration-responsive folding and unfolding transitions in graphene oxide liquid crystal phases. 2011. In Review

22. Bagri A, Mattevi C, Acik M, Chabal YJ, Chhowalla M, Shenoy VB. Structural evolution during the reduction of chemically derived graphene oxide. Nat Chem. 2010; 2:581–587. [PubMed: 20571578]

23. Nel AE, Madler L, Velegol D, Xia T, Hoek EM, Somasundaran P, Klaessig F, Castranova V, Thompson M. Understanding biophysicochemical interactions at the nano-bio interface. Nat Mater. 2009; 8:543–557. [PubMed: 19525947]

24. Wörle-Knirsch JM, Pulskamp K, Krug HF. Oops They Did It Again! Carbon Nanotubes Hoax Scientists in Viability Assays. Nano Letters. 2006; 6:1261–1268. [PubMed: 16771591]

25. Casey A, Herzog E, Davoren M, Lyng FM, Byrne HJ, Chambers G. Spectroscopic analysis confirms the interactions between single walled carbon nanotubes and various dyes commonly used to assess cytotoxicity. Carbon. 2007; 45:1425–1432.

26. Guo L, Von Dem Bussche A, Buechner M, Yan A, Kane AB, Hurt RH. Adsorption of essential micronutrients by carbon nanotubes and the implications for nanotoxicity testing. Small. 2008; 4:721–727. [PubMed: 18504717]

27. Monteiro-Riviere NA, Inman AO. Challenges for assessing carbon nanomaterial toxicity to the skin. Carbon. 2006; 44:1070–1078.

28. Liu X, Gurel V, Morris D, Murray DW, Zhitkovich A, Kane AB, Hurt RH. Bioavailability of Nickel in Single-Wall Carbon Nanotubes. Advanced Materials. 2007; 19:2790–2796.

29. Fenoglio I, Tomatis M, Lison D, Muller J, Fonseca A, Nagy JB, Fubini B. Reactivity of carbon nanotubes: free radical generation or scavenging activity? Free Radic Biol Med. 2006; 40:1227–1233. [PubMed: 16545691]

30. Zhang LL, Xiong Z, Zhao XS. Pillaring chemically exfoliated graphene oxide with carbon nanotubes for photocatalytic degradation of dyes under visible light irradiation. ACS Nano. 2010; 4:7030–7036. [PubMed: 21028785]

31. Poland CA, Duffin R, Kinloch I, Maynard A, Wallace WAH, Seaton A, Stone V, Brown S, MacNee W, Donaldson K. Carbon nanotubes introduced into the abdominal cavity of mice show asbestos-like pathogenicity in a pilot study. Nat Nano. 2008; 3:423–428.

32. Guo, F.; Huang, J.; Shenoy, V.; Hurt, R. Water actuated folding and unfolding transitions in graphene oxide mesogenic materials. 2011. Manuscrip in preparation

33. Patra N, Wang B, Kral P. Nanodroplet activated and guided folding of graphene nanostructures. Nano Lett. 2009; 9:3766–3771. [PubMed: 19852466]

34. Hasan SA, Rigueur JL, Harl RR, Krejci AJ, Gonzalo-Juan I, Rogers BR, Dickerson JH. Transferable Graphene Oxide Films with Tunable Microstructures. ACS Nano. 2010; 4:7367–7372. [PubMed: 21114272]

35. Hsieh CT, Chen WY. Water/oil repellency and work of adhesion of liquid droplets on graphene oxide and graphene surfaces. Surface and Coatings Technology. 2011; 205:4554–4561.

36. Yang ST, Chang Y, Wang H, Liu G, Chen S, Wang Y, Liu Y, Cao A. Folding/aggregation of graphene oxide and its application in Cu2+ removal. J Colloid Interface Sci. 2010; 351:122–127. [PubMed: 20705296]

NIH-PA Author Manuscript

NIH-PA Author Manuscript

NIH-PA Author Manuscript

37. Cote LJ, Kim F, Huang J. Langmuir-Blodgett assembly of graphite oxide single layers. J Am Chem Soc. 2009; 131:1043–1049. [PubMed: 18939796]
38. Sun X, Liu Z, Welsher K, Robinson JT, Goodwin A, Zaric S, Dai H. Nano-Graphene Oxide for Cellular Imaging and Drug Delivery. Nano Res. 2008; 1:203–212. [PubMed: 20216934]
39. Buford MC, Hamilton RF Jr, Holian A. A comparison of dispersing media for various engineered carbon nanoparticles. Part Fibre Toxicol. 2007; 4:6. [PubMed: 17655771]
40. Yang X, Wang Y, Huang X, Ma Y, Huang Y, Yang R, Duana H, Chen Y. Multi-functionalized graphene oxide based anticancer drug-carrier with dual-targeting function and pH-sensitivity. J Mater Chem. 2010; 21:3448–3454.
41. Huang P, Xu C, Lin J, Wang C, Wang X, Zhang C, Zhou X, Guo S, Cui D. Folic Acid-conjugated Graphene Oxide loaded with Photosensitizers for Targeting Photodynamic Therapy. Theranostics. 2011; 1:240–250. [PubMed: 21562631]
42. Yang ST, Chen S, Chang Y, Cao A, Liu Y, Wang H. Removal of methylene blue from aqueous solution by graphene oxide. J Colloid Interface Sci. 2011; 359:24–29. [PubMed: 21482424]
43. Sheng L, Ren J, Miao Y, Wang J, Wang E. PVP-coated graphene oxide for selective determination of ochratoxin A via quenching fluorescence of free aptamer. Biosens Bioelectron. 2011; 26:3494–3499. [PubMed: 21334186]
44. Liu Y, Liu C-y, Liu Y. Investigation on fluorescence quenching of dyes by graphite oxide and graphene. Applied Surface Science. 2011; 257:5513–5518.
45. Tung VC, Allen MJ, Yang Y, Kaner RB. High-throughput solution processing of large-scale graphene. Nat Nanotechnol. 2009; 4:25–29. [PubMed: 19119278]
46. Ren H, Wang C, Zhang J, Zhou X, Xu D, Zheng J, Guo S. DNA cleavage system of nanosized graphene oxide sheets and copper ions. ACS Nano. 2010; 4:7169–7174. [PubMed: 21082807]
47. Lu CH, Zhu CL, Li J, Liu JJ, Chen X, Yang HH. Using graphene to protect DNA from cleavage during cellular delivery. Chem Commun (Camb). 2010; 46:3116–3118. [PubMed: 20424750]
48. Wang Y, Li Z, Hu D, Lin CT, Li J, Lin Y. Aptamer/graphene oxide nanocomplex for in situ molecular probing in living cells. J Am Chem Soc. 2010; 132:9274–9276. [PubMed: 20565095]
49. Xu Y, Wu Q, Sun Y, Bai H, Shi G. Three-Dimensional Self-Assembly of Graphene Oxide and DNA into Multifunctional Hydrogels. ACS Nano. 2010; 4:7358–7362. [PubMed: 21080682]
50. Wu M, Kempaiah R, Huang PJ, Maheshwari V, Liu J. Adsorption and Desorption of DNA on Graphene Oxide Studied by Fluorescently Labeled Oligonucleotides. Langmuir. 2011; 27:2731–2738.
51. Titov AV, Kral P, Pearson R. Sandwiched graphene--membrane superstructures. ACS Nano. 2010; 4:229–234. [PubMed: 20025267]
52. Chen Y, Bothun GD. Lipid-assisted formation and dispersion of aqueous and bilayer-embedded nano-C60. Langmuir. 2009; 25:4875–4879. [PubMed: 19397348]
53. Wang B, Zhang L, Bae SC, Granick S. Nanoparticle-induced surface reconstruction of phospholipid membranes. Proc Natl Acad Sci U S A. 2008; 105:18171–18175. [PubMed: 19011086]
54. Zhang M, Yin BC, Wang XF, Ye BC. Interaction of peptides with graphene oxide and its application for real-time monitoring of protease activity. Chem Commun (Camb). 2011; 47:2399–2401. [PubMed: 21305066]
55. Qin W, Li X, Bian WW, Fan XJ, Qi JY. Density functional theory calculations and molecular dynamics simulations of the adsorption of biomolecules on graphene surfaces. Biomaterials. 2010; 31:1007–1016. [PubMed: 19880174]
56. Liu X, Sen S, Liu J, Kulaots I, Geohegan D, Kane A, Puretzky A, Rouleau C, More K, Palmore G, Hurt R. Antioxidant deactivation on graphenic nanocarbon surfaces. Small. 2011 in press.
57. Chang Y, Yang ST, Liu JH, Dong E, Wang Y, Cao A, Liu Y, Wang H. In vitro toxicity evaluation of graphene oxide on A549 cells. Toxicol Lett. 2011; 200:201–210. [PubMed: 21130147]
58. Donaldson K, Aitken R, Tran L, Stone V, Duffin R, Forrest G, Alexander A. Carbon Nanotubes: A Review of Their Properties in Relation to Pulmonary Toxicology and Workplace Safety. Toxicological Sciences. 2006; 92:5–22. [PubMed: 16484287]

NIH-PA Author Manuscript

NIH-PA Author Manuscript

NIH-PA Author Manuscript

59. Sanchez VC, Pietruska JR, Miselis NR, Hurt RH, Kane AB. Biopersistence and potential adverse health impacts of fibrous nanomaterials: what have we learned from asbestos? Wiley Interdisciplinary Reviews: Nanomedicine and Nanobiotechnology. 2009; 1:511–529. [PubMed: 20049814]
60. Liu X, Hurt RH, Kane AB. Biodurability of Single-Walled Carbon Nanotubes Depends on Surface Functionalization. Carbon N Y. 2010; 48:1961–1969. [PubMed: 20352066]
61. Allen BL, Kichambare PD, Gou P, Vlasova II, Kapralov AA, Konduru N, Kagan VE, Star A. Biodegradation of single-walled carbon nanotubes through enzymatic catalysis. Nano Lett. 2008; 8:3899–3903. [PubMed: 18954125]
62. Kagan VE, Konduru NV, Feng W, Allen BL, Conroy J, Volkov Y, Vlasova II, Belikova NA, Yanamala N, Kapralov A, Tyurina YY, Shi J, Kisin ER, Murray AR, Franks J, Stolz D, Gou P, Klein-Seetharaman J, Fadeel B, Star A, Shvedova AA. Carbon nanotubes degraded by neutrophil myeloperoxidase induce less pulmonary inflammation. Nat Nanotechnol. 2010; 5:354–359. [PubMed: 20364135]
63. Kotchey GP, Allen BL, Vedala H, Yanamala N, Kapralov AA, Tyurina YY, Klein-Seetharaman J, Kagan VE, Star A. The enzymatic oxidation of graphene oxide. ACS Nano. 2011; 5:2098–2108. [PubMed: 21344859]
64. Yan L, Zhao F, Li S, Hu Z, Zhao Y. Low-toxic and safe nanomaterials by surface-chemical design, carbon nanotubes, fullerenes, metallofullerenes, and graphenes. Nanoscale. 2011; 3:362–382. [PubMed: 21157592]
65. Ibald-Mulli A, Wichmann HE, Kreyling W, Peters A. Epidemiological evidence on health effects of ultrafine particles. J Aerosol Med. 2002; 15:189–201. [PubMed: 12184869]
66. Pope CA 3rd. Air pollution and health - good news and bad. N Engl J Med. 2004; 351:1132–1134. [PubMed: 15356311]
67. Schulz H, Harder V, Ibald-Mulli A, Khandoga A, Koenig W, Krombach F, Radykewicz R, Stampfl A, Thorand B, Peters A. Cardiovascular effects of fine and ultrafine particles. J Aerosol Med. 2005; 18:1–22. [PubMed: 15741770]
68. ICRP. Publication 66: Human Respiratory Tract Model for Radiological Protection. Vol. 24. Elsevier Science, Inc; Tarrytown, New York: 1994.
69. NCRP. Deposition, retention and dosimetry of inhaled radioactive substances. National Council on Radiation Protection and Measurements; Bethesda, MD: 1994.
70. Hinds, W. Aerosol Technology: Properties, Behavior, and Measurement of Airborne Particles. 2. Wiley-Interscience; New York: 1999.
71. Itoh H, Nishino M, Hatabu H. Architecture of the lung: morphology and function. J Thorac Imaging. 2004; 19:221–227. [PubMed: 15502608]
72. Matthews LW, Spector S, Lemm J, Potter JL. Studies on Pulmonary Secretions. I. The over-All Chemical Composition of Pulmonary Secretions from Patients with Cystic Fibrosis, Bronchiectasis, and Laryngectomy. Am Rev Respir Dis. 1963; 88:199–204. [PubMed: 14045224]
73. Phipps RJ. Production of Airway Secretions. Semin Respir Med. 1984; 5:314–318.
74. Sheehan JK, Thornton DJ, Somerville M, Carlstedt I. Mucin structure. The structure and heterogeneity of respiratory mucus glycoproteins. Am Rev Respir Dis. 1991; 144:S4–9. [PubMed: 1892325]
75. Roussel P, Lamblin G, Lhermitte M, Houdret N, Lafitte JJ, Perini JM, Klein A, Scharfman A. The complexity of mucins. Biochimie. 1988; 70:1471–1482. [PubMed: 3149516]
76. Samet JM, Cheng PW. The role of airway mucus in pulmonary toxicology. Environ Health Perspect. 1994; 102(Suppl 2):89–103. [PubMed: 7925190]
77. Cheng YS, Yeh HC, Allen MD. Dynamic Shape Factor of a Plate-Like Particle. Aerosol Sci Tech. 1988; 8:109–123.
78. Cone RA. Barrier properties of mucus. Adv Drug Deliv Rev. 2009; 61:75–85. [PubMed: 19135107]
79. Lai SK, Wang YY, Hanes J. Mucus-penetrating nanoparticles for drug and gene delivery to mucosal tissues. Adv Drug Deliv Rev. 2009; 61:158–171. [PubMed: 19133304]
80. Hummer G, Rasaiah JC, Noworyta JP. Water conduction through the hydrophobic channel of a carbon nanotube. Nature. 2001; 414:188–190. [PubMed: 11700553]

NIH-PA Author Manuscript

NIH-PA Author Manuscript

NIH-PA Author Manuscript

81. Lai SK, O'Hanlon DE, Harrold S, Man ST, Wang YY, Cone R, Hanes J. Rapid transport of large polymeric nanoparticles in fresh undiluted human mucus. Proc Natl Acad Sci U S A. 2007; 104:1482–1487. [PubMed: 17244708]
82. Li B, Logan BE. Bacterial adhesion to glass and metal-oxide surfaces. Colloids Surf B Biointerfaces. 2004; 36:81–90. [PubMed: 15261011]
83. Tang BC, Dawson M, Lai SK, Wang YY, Suk JS, Yang M, Zeitlin P, Boyle MP, Fu J, Hanes J. Biodegradable polymer nanoparticles that rapidly penetrate the human mucus barrier. Proc Natl Acad Sci U S A. 2009; 106:19268–19273. [PubMed: 19901335]
84. Wang YY, Lai SK, So C, Schneider C, Cone R, Hanes J. Mucoadhesive nanoparticles may disrupt the protective human mucus barrier by altering its microstructure. PLoS One. 2011; 6:e21547. [PubMed: 21738703]
85. Green, F.; Churg, A. Chapter 8: Pathology of Occupational Lung Disease. 2. Williams & Wilkins; Baltimore: 1998. Diseases due to nonasbestos silicates.
86. Mukhopadhyay S, Gal AA. Granulomatous lung disease: an approach to the differential diagnosis. Arch Pathol Lab Med. 2010; 134:667–690. [PubMed: 20441499]
87. Kunkel SL, Lukacs NW, Strieter RM, Chensue SW. Animal models of granulomatous inflammation. Semin Respir Infect. 1998; 13:221–228. [PubMed: 9764953]
88. Card JW, Zeldin DC, Bonner JC, Nestmann ER. Pulmonary applications and toxicity of engineered nanoparticles. Am J Physiol Lung Cell Mol Physiol. 2008; 295:L400–411. [PubMed: 18641236]
89. Kang S, Pinault M, Pfefferle LD, Elimelech M. Single-walled carbon nanotubes exhibit strong antimicrobial activity. Langmuir. 2007; 23:8670–8673. [PubMed: 17658863]
90. Kang S, Herzberg M, Rodrigues DF, Elimelech M. Antibacterial effects of carbon nanotubes: size does matter! Langmuir. 2008; 24:6409–6413. [PubMed: 18512881]
91. Akhavan O, Ghaderi E. Toxicity of graphene and graphene oxide nanowalls against bacteria. ACS Nano. 2010; 4:5731–5736. [PubMed: 20925398]
92. Hu W, Peng C, Luo W, Lv M, Li X, Li D, Huang Q, Fan C. Graphene-based antibacterial paper. ACS Nano. 2010; 4:4317–4323. [PubMed: 20593851]
93. Tazawa H, Tatemichi M, Sawa T, Gilibert I, Ma N, Hiraku Y, Donehower LA, Ohgaki H, Kawanishi S, Ohshima H. Oxidative and nitrative stress caused by subcutaneous implantation of a foreign body accelerates sarcoma development in Trp53+/− mice. Carcinogenesis. 2007; 28:191–198. [PubMed: 16857722]
94. Wang G, Qian F, Saltikov CW, Jiao Y, Li Y. Microbial reduction of graphene oxide by *Shewanella*. Nano Res. 2011; 4:563–570.
95. Williams LB, Metge DW, Eberl DD, Harvey RW, Turner AG, Prapaipong P, Poret-Peterson AT. What makes a natural clay antibacterial? Environ Sci Technol. 2011; 45:3768–3773. [PubMed: 21413758]
96. Muller J, Huaux F, Moreau N, Misson P, Heilier JF, Delos M, Arras M, Fonseca A, Nagy JB, Lison D. Respiratory toxicity of multi-wall carbon nanotubes. Toxicol Appl Pharmacol. 2005; 207:221–231. [PubMed: 16129115]
97. Sanchez VC, Weston P, Yan A, Hurt RH, Kane AB. A 3-dimensional in vitro model of epithelioid granulomas induced by high aspect ratio nanomaterials. Part Fibre Toxicol. 2011; 8:17. [PubMed: 21592387]
98. Wang K, Ruan J, Song H, Zhang J, Wo Y, Guo S, Cui D. Biocompatibility of Graphene Oxide. Nanoscale Res Lett. 2011; 6:8.
99. Zhang Y, Ali SF, Dervishi E, Xu Y, Li Z, Casciano D, Biris AS. Cytotoxicity Effects of Graphene and Single-Wall Carbon Nanotubes in Neural Phaeochromocytoma-Derived PC12 Cells. ACS Nano. 2010; 4:3181–3186. [PubMed: 20481456]
100. Hu W, Peng C, Lv M, Li X, Zhang Y, Chen N, Fan C, Huang Q. Protein corona-mediated mitigation of cytotoxicity of graphene oxide. ACS Nano. 2011; 5:3693–3700. [PubMed: 21500856]
101. Sasidharan A, Panchakarla LS, Chandran P, Menon D, Nair S, Rao CNR, Koyakutty M. Differential nano-bio interactions and toxicity effects of pristine versus functionalized graphene. Nanoscale. 2011; 3:2461–2464. [PubMed: 21562671]

NIH-PA Author Manuscript

NIH-PA Author Manuscript

NIH-PA Author Manuscript

102. Oberdörster G, Oberdörster E, Oberdörster J. Nanotoxicology: an emerging discipline evolving from studies of ultrafine particles. Environ Health Perspect. 2005; 113:823–839. [PubMed: 16002369]
103. Stone V, Johnston H, Schins RPF. Development of in vitro systems for nanotoxicology: methodological considerations. Critical Reviews in Toxicology. 2009; 39:613–626. [PubMed: 19650720]
104. Yang K, Zhang S, Zhang G, Sun X, Lee ST, Liu Z. Graphene in mice: ultrahigh in vivo tumor uptake and efficient photothermal therapy. Nano Lett. 2010; 10:3318–3323. [PubMed: 20684528]
105. Yang K, Wan J, Zhang S, Zhang Y, Lee ST, Liu Z. In vivo pharmacokinetics, long-term biodistribution, and toxicology of PEGylated graphene in mice. ACS Nano. 2011; 5:516–522. [PubMed: 21162527]
106. Zhang X, Yin J, Peng C, Hu W, Zhu Z, Li W, Fan C, Huang Q. Distribution and biocompatibility studies of graphene oxide in mice after intravenous administration. Carbon. 2011; 49:986–995.
107. IARC. Monographs on the Evaluation of Carcinogenic Risks to Humans. Surgical Implants and Other Foreign Bodies. Vol. 74. International Agency for Research on Cancer/World Health Organization; Lyon, France: 1999.
108. Oppenheimer ET, Willhite M, Danishefsky I, Stout AP. Observations on the effects of powdered polymer in the carcinogenic process. Cancer Res. 1961; 21:132–134. [PubMed: 13731054]
109. Bischoff F, Bryson G. Carcinogenesis through solid state surfaces. Prog Exp Tumor Res. 1964; 5:85–133. [PubMed: 14317768]
110. Brand KG, Buoen LC, Brand I. Foreign-body tumorigenesis induced by glass and smooth and rough plastic. Comparative study of preneoplastic events. J Natl Cancer Inst. 1975; 55:319–322. [PubMed: 1159820]
111. Choi J, Curtis SJ, Roy DM, Flesken-Nikitin A, Nikitin AY. Local mesenchymal stem/progenitor cells are a preferential target for initiation of adult soft tissue sarcomas associated with p53 and Rb deficiency. Am J Pathol. 2010; 177:2645–2658. [PubMed: 20864684]
112. Okada F. Beyond foreign-body-induced carcinogenesis: impact of reactive oxygen species derived from inflammatory cells in tumorigenic conversion and tumor progression. Int J Cancer. 2007; 121:2364–2372. [PubMed: 17893867]
113. Soldano C, Mahmood A, Dujardin E. Production, properties and potential of graphene. Carbon. 2010; 48:2127–2150.
114. Brand KG, Buoen LC, Johnson KH, Brand I. Etiological factors, stages, and the role of the foreign body in foreign body tumorigenesis: a review. Cancer Res. 1975; 35:279–286. [PubMed: 1089044]
115. Kirkpatrick CJ, Alves A, Kohler H, Kriegsmann J, Bittinger F, Otto M, Williams DF, Eloy R. Biomaterial-induced sarcoma: A novel model to study preneoplastic change. Am J Pathol. 2000; 156:1455–1467. [PubMed: 10751369]
116. James SJ, Pogribna M, Miller BJ, Bolon B, Muskhelishvili L. Characterization of cellular response to silicone implants in rats: implications for foreign-body carcinogenesis. Biomaterials. 1997; 18:667–675. [PubMed: 9151998]
117. Balkwill F, Mantovani A. Inflammation and cancer: back to Virchow? Lancet. 2001; 357:539–545. [PubMed: 11229684]
118. Ohshima H. Genetic and epigenetic damage induced by reactive nitrogen species: implications in carcinogenesis. Toxicol Lett. 2003; 140–141:99–104.
119. Allen BL, Kotchey GP, Chen Y, Yanamala NV, Klein-Seetharaman J, Kagan VE, Star A. Mechanistic investigations of horseradish peroxidase-catalyzed degradation of single-walled carbon nanotubes. J Am Chem Soc. 2009; 131:17194–17205. [PubMed: 19891488]
120. Chun YW, Wang W, Choi J, Nam TH, Lee YH, Cho KK, Im YM, Kim M, Gwon YH, Kang SS, Lee JD, Lee K, Khang D, Webster TJ. Control of macrophage responses on hydrophobic and hydrophilic carbon nanostructures. Carbon. 2011; 49:2092–2103.
121. Nayak TR, Andersen H, Makam VS, Khaw C, Bae S, Xu X, Ee PL, Ahn JH, Hong BH, Pastorin G, Ozyilmaz B. Graphene for Controlled and Accelerated Osteogenic Differentiation of Human Mesenchymal Stem Cells. ACS Nano. 2011; 5:4670–4678. [PubMed: 21528849]

NIH-PA Author Manuscript

NIH-PA Author Manuscript

NIH-PA Author Manuscript

122. Kalbacova M, Broz A, Kong J, Kalbac M. Graphene substrates promote adherence of human osteoblasts and mesenchymal stromal cells. Carbon. 2010; 48:4323–4329.
123. Feng L, Zhang S, Liu Z. Graphene based gene transfection. Nanoscale. 2011; 3:1252–1257. [PubMed: 21270989]
124. Rana VK, Choi MC, Kong JY, Kim GY, Kim MJ, Kim SH, Mishra S, Singh RP, Ha CS. Chitosan-Functionalized Graphene Oxide Hybrid Nanosheets. Macromol Mater Eng. 2011; 296:131–140.
125. Depan D, Shah JS, Misra RD. Controlled release of drug from folate-decorated and graphene mediated drug delivery system: Synthesis, loading effciency, and drug release response. Materials Science and Engineering C. 2011 in press.
126. Liu Z, Robinson JT, Sun X, Dai H. PEGylated nanographene oxide for delivery of water-insoluble cancer drugs. J Am Chem Soc. 2008; 130:10876–10877. [PubMed: 18661992]
127. Yang X, Zhang X, Liu Z, Ma Y, Huang Y, Chen Y. High-Efficiency Loading and Controlled Release of Doxorubicin Hydrochloride on Graphene Oxide. The Journal of Physical Chemistry C. 2008; 112:17554–17558.
128. Abdali A, Moritz B, Gupta A, Wiggers H, Schulz C. Hybrid microwave-plasma hot-wall reactor for synthesis of silica nanoparticles under well-controlled conditions. J Optoelectron Adv M. 2010; 12:440–444.
129. Motta G, Cea M, Moran E, Carbone F, Augusti V, Patrone F, Nencioni A. Monoclonal antibodies for non-Hodgkin's lymphoma: state of the art and perspectives. Clin Dev Immunol. 2010; 2010:428253. [PubMed: 21437222]
130. Bai JP. Ongoing challenges in drug interaction safety: from exposure to pharmacogenomics. Drug Metab Pharmacokinet. 2010; 25:62–71. [PubMed: 20208389]
131. O'Connor AE, Gallagher WM, Byrne AT. Porphyrin and nonporphyrin photosensitizers in oncology: preclinical and clinical advances in photodynamic therapy. Photochem Photobiol. 2009; 85:1053–1074. [PubMed: 19682322]
132. Frank IW, Tanenbaum DM, van der Zande AM, McEuen PL. Mechanical properties of suspended graphene sheets. The Journal of Vacuum Science and Technology B. 2007; 25:2558–2561.
133. Lee C, Wei X, Kysar JW, Hone J. Measurement of the elastic properties and intrinsic strength of monolayer graphene. Science. 2008; 321:385–388. [PubMed: 18635798]
134. Lee Y, Bae S, Jang H, Jang S, Zhu SE, Sim SH, Song YI, Hong BH, Ahn JH. Wafer-scale synthesis and transfer of graphene films. Nano Lett. 2010; 10:490–493. [PubMed: 20044841]
135. Drury JL, Mooney DJ. Hydrogels for tissue engineering: scaffold design variables and applications. Biomaterials. 2003; 24:4337–4351. [PubMed: 12922147]
136. Gkioni K, Leeuwenburgh SC, Douglas TE, Mikos AG, Jansen JA. Mineralization of hydrogels for bone regeneration. Tissue Eng Part B Rev. 2010; 16:577–585. [PubMed: 20735319]
137. Kloxin AM, Kloxin CJ, Bowman CN, Anseth KS. Mechanical properties of cellularly responsive hydrogels and their experimental determination. Adv Mater. 2010; 22:3484–3494. [PubMed: 20473984]
138. Liang BJ, Huang Y, Zhang L, Wang Y, Ma Y, Guo T, Chen Y. Molecular-Level Dispersion of Graphene into Poly(vinyl alcohol) and Effective Reinforcement of their Nanocomposites. Advanced Functional Materials. 2009; 19:2297–2302.
139. Zhang L, Wang Z, Xu C, Li Y, Gao J, Wangc W, Liu Y. High strength graphene oxide/polyvinyl alcohol composite hydrogels. J Mater Chem. 2011 in press.
140. Ramanathan T, Abdala AA, Stankovich S, Dikin DA, Herrera-Alonso M, Piner RD, Adamson DH, Schniepp HC, Chen X, Ruoff RS, Nguyen ST, Aksay IA, Prud'Homme RK, Brinson LC. Functionalized graphene sheets for polymer nanocomposites. Nat Nanotechnol. 2008; 3:327–331. [PubMed: 18654541]
141. Das B, Eswar Prasad K, Ramamurty U, Rao CN. Nano-indentation studies on polymer matrix composites reinforced by few-layer graphene. Nanotechnology. 2009; 20:125705. [PubMed: 19420482]
142. Di Martino A, Sittinger M, Risbud MV. Chitosan: a versatile biopolymer for orthopaedic tissue-engineering. Biomaterials. 2005; 26:5983–5990. [PubMed: 15894370]

NIH-PA Author Manuscript

NIH-PA Author Manuscript

NIH-PA Author Manuscript

143. Berger J, Reist M, Mayer JM, Felt O, Gurny R. Structure and interactions in chitosan hydrogels formed by complexation or aggregation for biomedical applications. Eur J Pharm Biopharm. 2004; 57:35–52. [PubMed: 14729079]

144. Fan H, Wang L, Zhao K, Li N, Shi Z, Ge Z, Jin Z. Fabrication, Mechanical Properties, and Biocompatibility of Graphene-Reinforced Chitosan Composites. Biomacromolecules. 2010; 11:2345–2351. [PubMed: 20687549]

145. Depan D, Girase B, Shah JS, Misra RD. Structure-process-property relationship of the polar graphene oxide-mediated cellular response and stimulated growth of osteoblasts on hybrid chitosan network structure nanocomposite scaffolds. Acta Biomater. 2011; 7:3432–3445. [PubMed: 21664303]

146. Kodali VK, Scrimgeour J, Kim S, Hankinson JH, Carroll KM, de Heer WA, Berger C, Curtis JE. Nonperturbative chemical modification of graphene for protein micropatterning. Langmuir. 2011; 27:863–865. [PubMed: 21182241]

147. Chen RJ, Zhang Y, Wang D, Dai H. Noncovalent sidewall functionalization of single-walled carbon nanotubes for protein immobilization. J Am Chem Soc. 2001; 123:3838–3839. [PubMed: 11457124]

148. Nair RR, Blake P, Blake JR, Zan R, Anissimova S, Bangert U, Golovanov AP, Morozov SV, Geim AK, Novoselov KS, Latychevskaia T. Graphene as a transparent conductive support for studying biological molecules by transmission electron microscopy. journal article. 2010; 97:153102–153105.

149. Heo C, Yoo J, Lee S, Jo A, Jung S, Yoo H, Lee YH, Suh M. The control of neural cell-to-cell interactions through non-contact electrical field stimulation using graphene electrodes. Biomaterials. 2011; 32:19–27. [PubMed: 20880583]

150. Nelson T, Zhang B, Prezhdo OV. Detection of nucleic acids with graphene nanopores: ab initio characterization of a novel sequencing device. Nano Lett. 2010; 10:3237–3242. [PubMed: 20722409]

151. Salas EC, Sun Z, Luttge A, Tour JM. Reduction of graphene oxide via bacterial respiration. ACS Nano. 2010; 4:4852–4856. [PubMed: 20731460]

152. Cui Y, Kim SN, Jones SE, Wissler LL, Naik RR, McAlpine MC. Chemical functionalization of graphene enabled by phage displayed peptides. Nano Lett. 2010; 10:4559–4565. [PubMed: 20942387]

153. Peng C, Hu W, Zhou Y, Fan C, Huang Q. Intracellular imaging with a graphene-based fluorescent probe. Small. 2010; 6:1686–1692. [PubMed: 20602429]

154. Li Y, Zhou X, Ye D. Molecular beacons: an optimal multifunctional biological probe. Biochem Biophys Res Commun. 2008; 373:457–461. [PubMed: 18489905]

155. Hamilton, C. Rice University. Houston, TX: 2009.

156. Blanchard KT, Barthel C, French JE, Holden HE, Moretz R, Pack FD, Tennant RW, Stoll RE. Transponder-Induced Sarcoma in the Heterozygous p53+/− Mouse. Toxicologic Pathology. 1999; 27:519–527. [PubMed: 10528631]

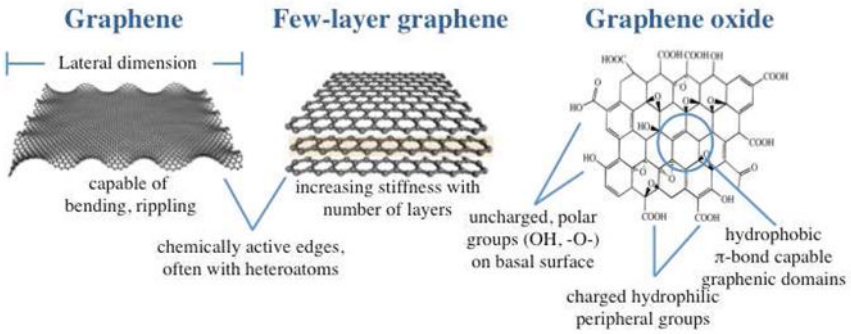

Figure 1.

Example members of the graphene nanomaterial family and selected properties relevant to colloidal behavior and biological interactions. Graphene oxide sketch adapted with permission from Hamilton [155].

NIH-PA Author Manuscript
NIH-PA Author Manuscript
NIH-PA Author Manuscript

NIH-PA Author Manuscript

NIH-PA Author Manuscript

NIH-PA Author Manuscript

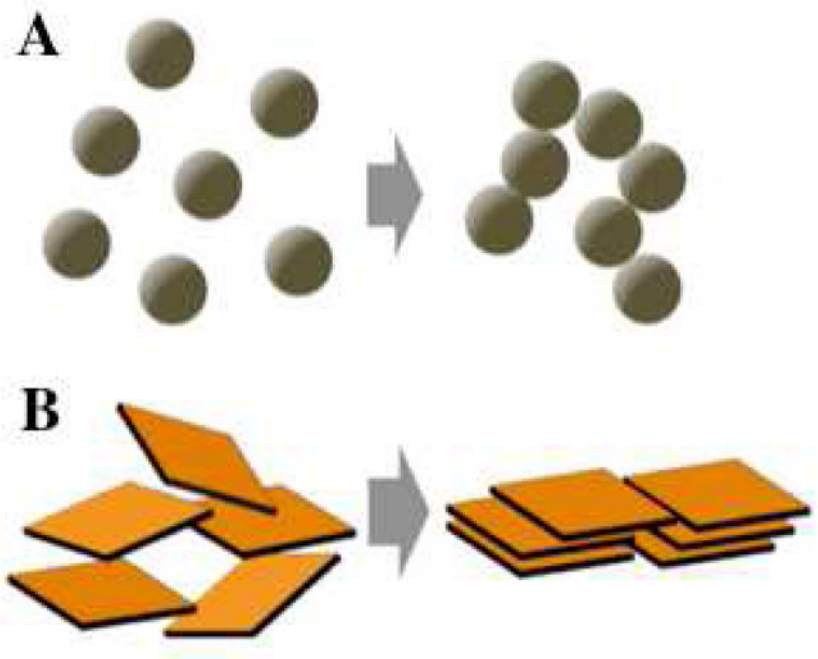

Figure 2.

Surface area stability during aggregation, filtration, or drying for spherical (A) and plate-like (B) particles. Sphere-to-sphere point contact preserves most surface area, but plate alignment destroys surface area if interlayer spaces are inaccessible to adsorbates or surface area measurement probes. This is the case for most GFNs, where interlayer spacing ranges from 0.34 nm – 1 nm, which is too small even for N_2 penetration used in BET analysis.

NIH-PA Author Manuscript

NIH-PA Author Manuscript

NIH-PA Author Manuscript

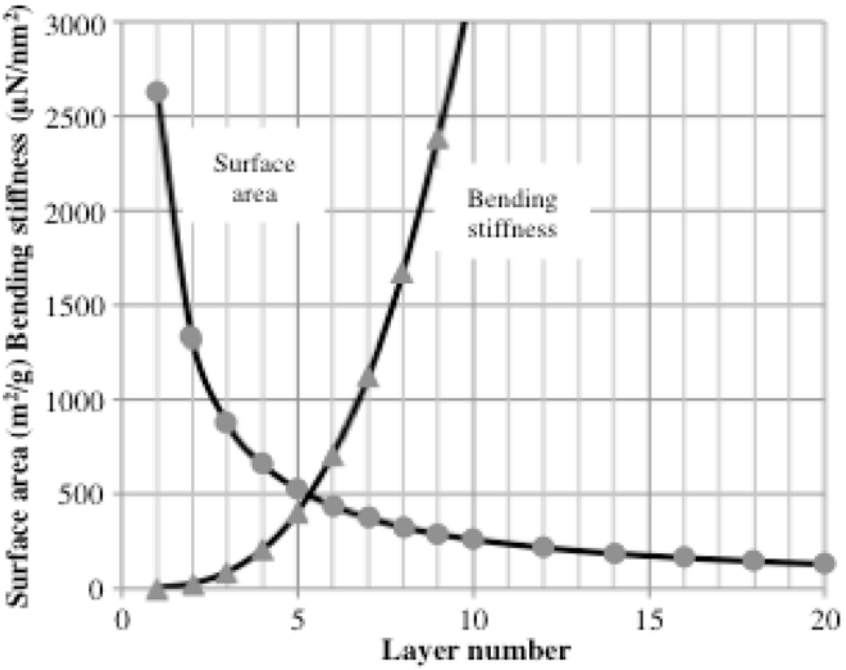

Figure 3.

Surface area and bending stiffness for ideal GFNs, calculated from geometry and using 1 TPa for the elastic modulus of a graphene sheet [133] and the area moment of inertia for multilayer materials with interlayer spacing of 0.34 nm.

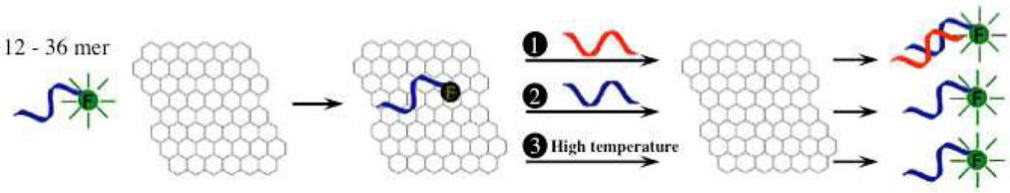

Figure 4.

Adsorption and quenching of dye-labeled DNA on graphene surfaces, and its (1) desorption in presence of c-DNA, (2) exchange with the same DNA in solution, or limited desorption upon increasing temperature up to 95 ° C. Note that the experiments involve GO, but the structure shown is that of graphene, and can be taken to represent the unmodified hydrophobic patches on GO surfaces. Figure adapted from Wu *et al.* [49] with permission.

NIH-PA Author Manuscript NIH-PA Author Manuscript NIH-PA Author Manuscript

NIH-PA Author Manuscript

NIH-PA Author Manuscript

NIH-PA Author Manuscript

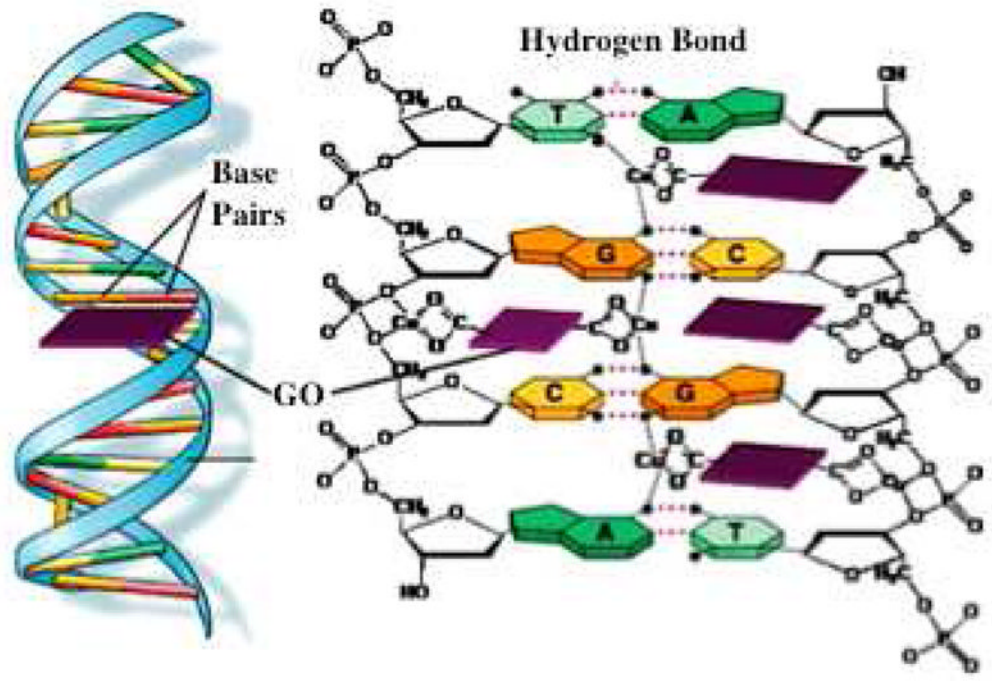

Figure 5.
DNA cleavage mechanism involving intercalation by GO/Cu^{2+}. Figure from Ren *et al.* [46] used by permission.

NIH-PA Author Manuscript

NIH-PA Author Manuscript

NIH-PA Author Manuscript

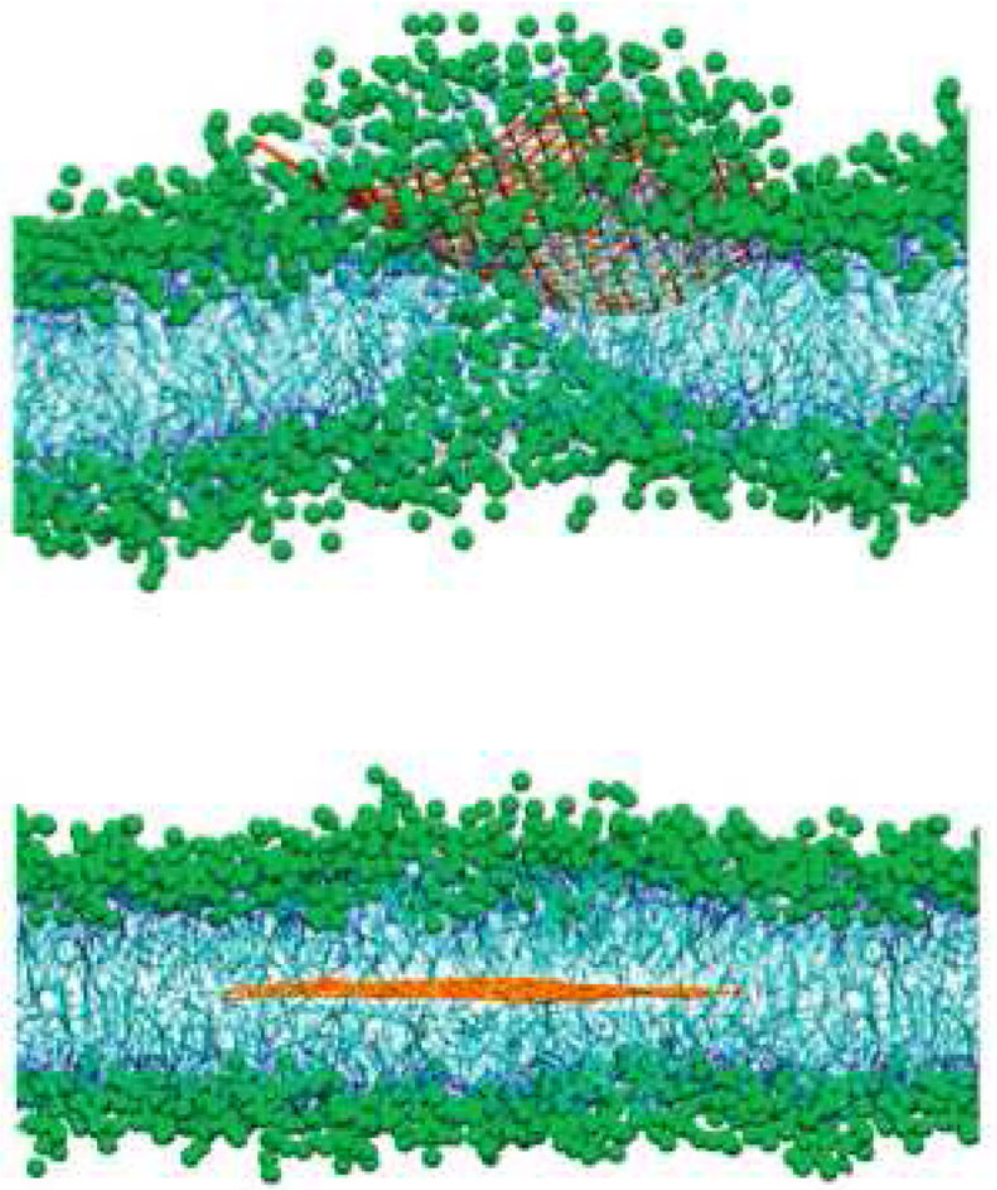

Figure 6.

Molecular dynamics simulations showing fusion of lipid-coated monolayer graphene with a lipid bilayer, leading to localization of the sheet in the interleaflet hydrophobic core. Left: intermediate stage of fusion and entry: Right: stable imbedding in hydrophobic core. Figure adapted from Titov *et al.* [51] and reprinted with permission.

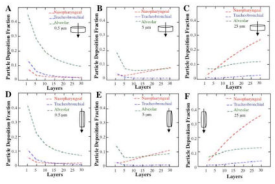

Figure 7.
Regional fractional deposition of GFNs in the human respiratory tract. Figures A–C provide particle deposition fractions for particles moving along the polar axis whereas figures D–F provide particle deposition fractions for particles moving perpendicular to the polar axis (A–C) Deposition of 0.5, 5 and 25 μm sized FLGs in the nasopharyngeal, tracheobronchial and alveolar regions respectively; (D–F) Deposition of 0.5, 5 and 25 μm sized FLGs in the nasopharyngeal, tracheobronchial and alveolar regions respectively.

NIH-PA Author Manuscript
NIH-PA Author Manuscript
NIH-PA Author Manuscript

NIH-PA Author Manuscript
NIH-PA Author Manuscript
NIH-PA Author Manuscript

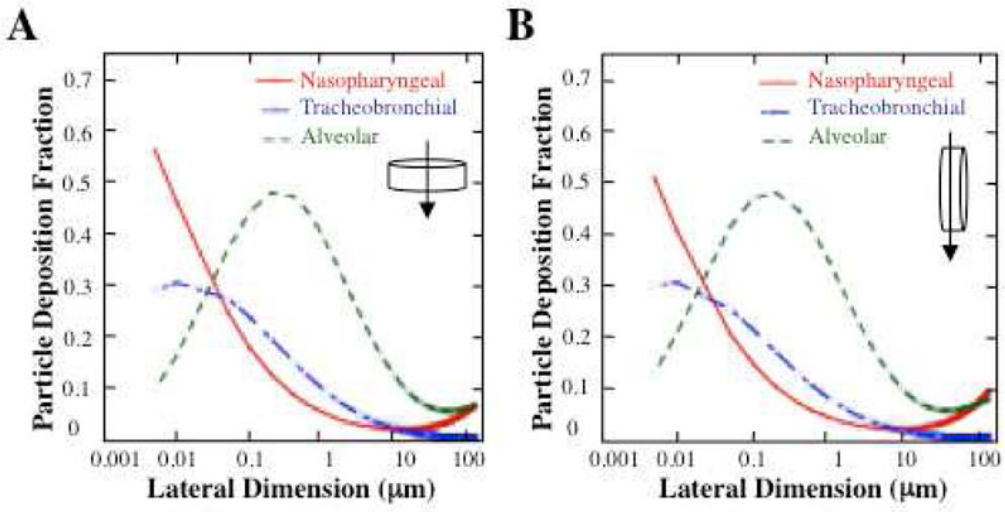

Figure 8.

Regional fractional deposition of GFNs in the nasopharyngeal, tracheobronchial and alveolar regions of the human respiratory tract. Lateral dimension ranges from 5 nm to 100 μm. Particles are assumed to be 1 layer thick; layer thickness = 0.34 nm. (A) Particle deposition as the particle moves along the polar axis; and (B) particle deposition as the particle moves perpendicular to the polar axis.

NIH-PA Author Manuscript
NIH-PA Author Manuscript
NIH-PA Author Manuscript

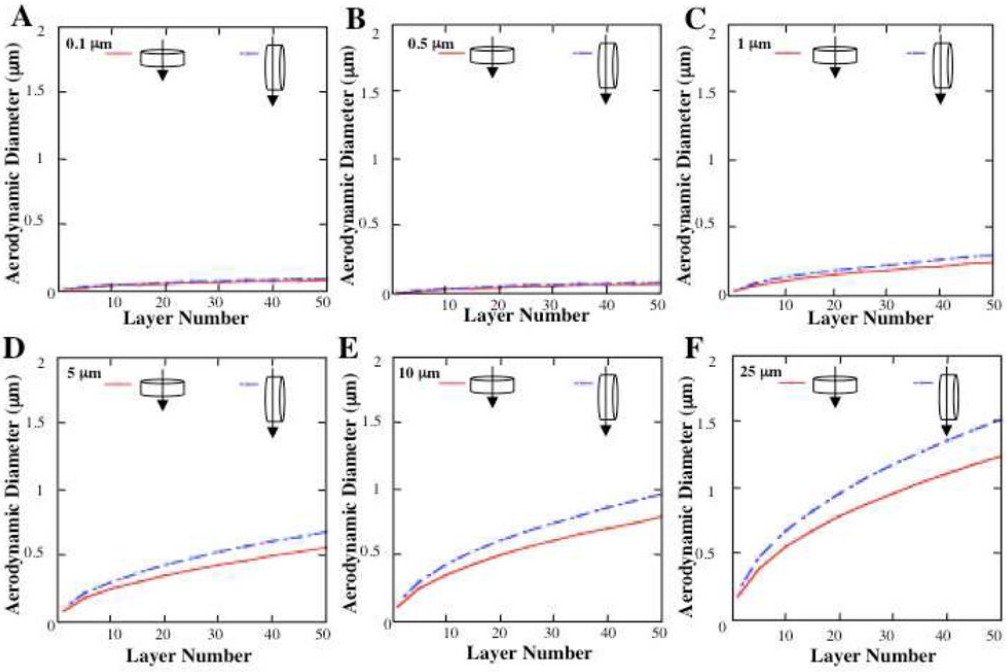

Figure 9.

Aerodynamic diameter of various GFNs as a function of layer number. Aerodynamic diameters were determined using two different orientations: (1) particle moves along the polar axis [27]; and (2) particle moves perpendicular to the polar axis (BLUE).

NIH-PA Author Manuscript

NIH-PA Author Manuscript

NIH-PA Author Manuscript

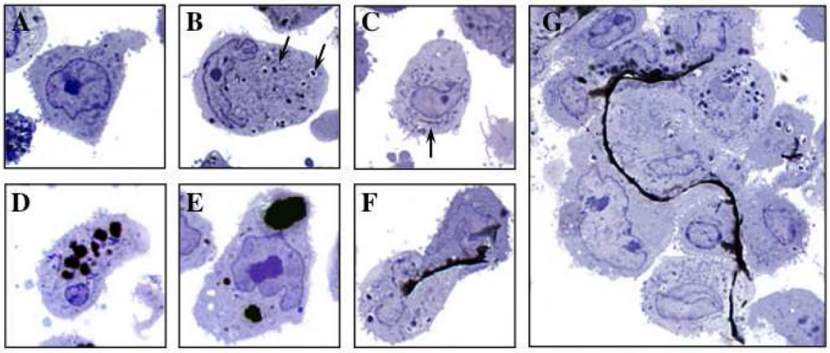

Figure 10.

Size-dependent internalization of FLG by human THP-1 macrophages. Untreated cells (A) or cells exposed to 1μg/ml of carbon black particles (B), multi-walled carbon nanotubes (C), or FLG with increasing lateral size: 550 nm (D), 800 nm (E), 5μm (F) or 25 μm (G). Cells were fixed after 24 hrs of exposure, embedded in plastic, and 0.5 μm sections were stained with toluidine blue for light microscopy. Magnification: 1000X.

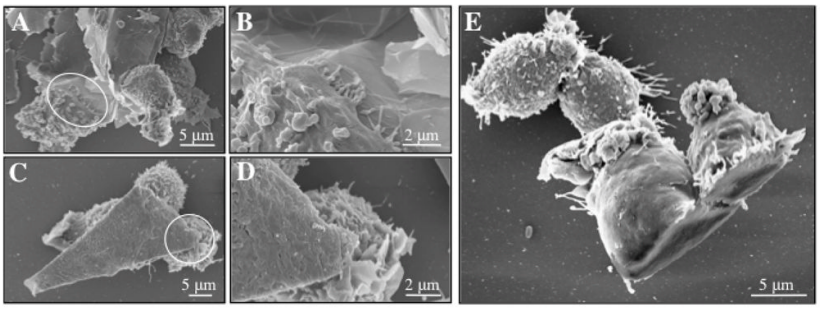

Figure 11.
Cellular interaction of macrophage with FLG. Following cellular recognition and attachment to FLG with 25 μm of lateral size (A–B), macrophages spread on and wrap the sheets (C–E) without perturbation of their plate-like shape.

NIH-PA Author Manuscript
NIH-PA Author Manuscript
NIH-PA Author Manuscript

NIH-PA Author Manuscript

NIH-PA Author Manuscript

NIH-PA Author Manuscript

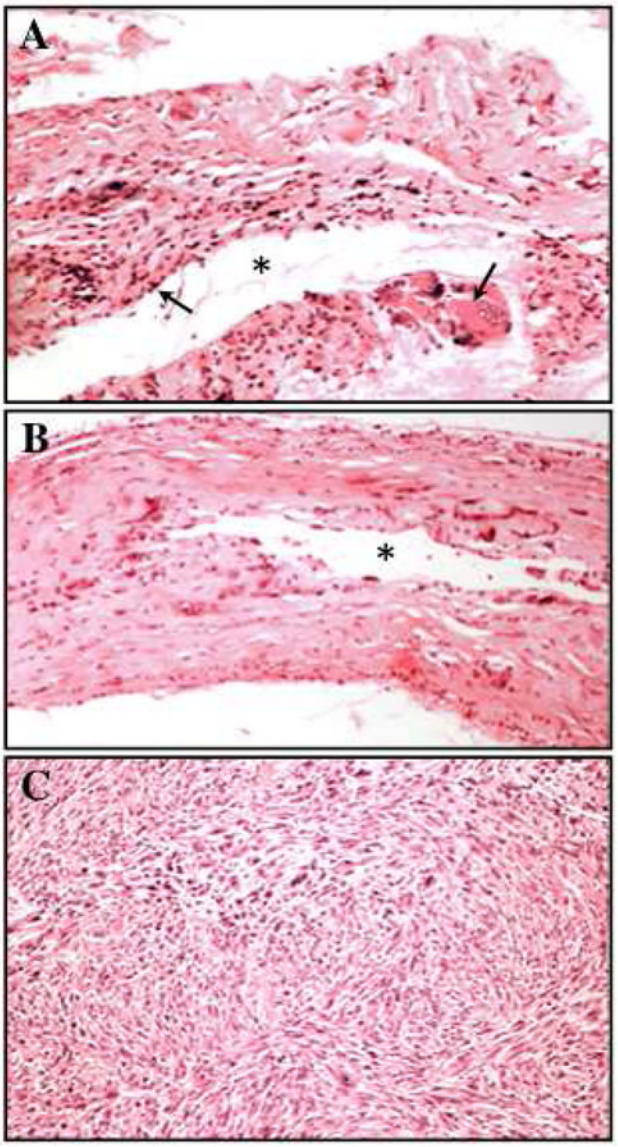

Figure 12.

Host response to subcutaneous implants in mice. Subcutaneous implantation of glass/polypropylene transponder identification devices has been shown to induce foreign body sarcomas in heterozygous p53-deficent mice [156]. The initial histopathological reaction (A) to the implant is accumulation of inflammatory cells characterized as macrophages and multinucleated giant cells. The implant becomes surrounded by a dense collagen capsule (B) containing scattered atypical fibroblasts. Atypical cells are large, irregular in shape, and have prominent nuclei. The implant (*) was removed before tissue processing. Foreign body sarcoma (C) composed of densely-packed fibroblast-like cells arranged in whorls. Light microscopy, hematoxylin and eosin stain. Magnification: 200X.